

740
5/25/79

Ln 2609

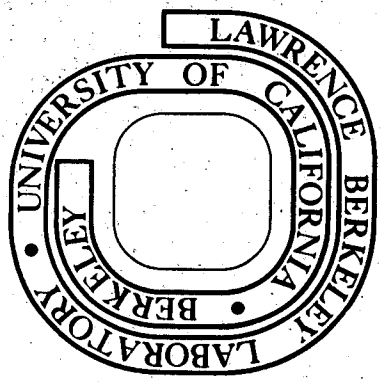
LBL-7076
UC-66a

SIMULATION OF THE KRAFLA GEOHERMAL FIELD

V. Jonsson

August 1978

MASTER



Prepared for the U.S. Department of Energy under
Contract No. W-7405-ENG-48

LEGAL NOTICE

This report was prepared as an account of work sponsored by the United States Government. Neither the United States nor the United States Department of Energy, nor any of their employees, nor any of their contractors, subcontractors, or their employees, makes any warranty, express or implied, or assumes any legal liability or responsibility for the accuracy, completeness or usefulness of any information, apparatus, product or process disclosed, or represents that its use would not infringe privately owned rights.

Printed in the United States of America

Available from

National Technical Information Service

U.S. Department of Commerce

5285 Port Royal Road

Springfield, VA 22161

Price Code: A04

DISCLAIMER

This report was prepared as an account of work sponsored by an agency of the United States Government. Neither the United States Government nor any agency Thereof, nor any of their employees, makes any warranty, express or implied, or assumes any legal liability or responsibility for the accuracy, completeness, or usefulness of any information, apparatus, product, or process disclosed, or represents that its use would not infringe privately owned rights. Reference herein to any specific commercial product, process, or service by trade name, trademark, manufacturer, or otherwise does not necessarily constitute or imply its endorsement, recommendation, or favoring by the United States Government or any agency thereof. The views and opinions of authors expressed herein do not necessarily state or reflect those of the United States Government or any agency thereof.

DISCLAIMER

Portions of this document may be illegible in electronic image products. Images are produced from the best available original document.

SIMULATION OF THE KRAFLA GEOTHERMAL FIELD*

V. Jonsson

Earth Sciences Division
Lawrence Berkeley Laboratory
University of California
Berkeley, California 94720

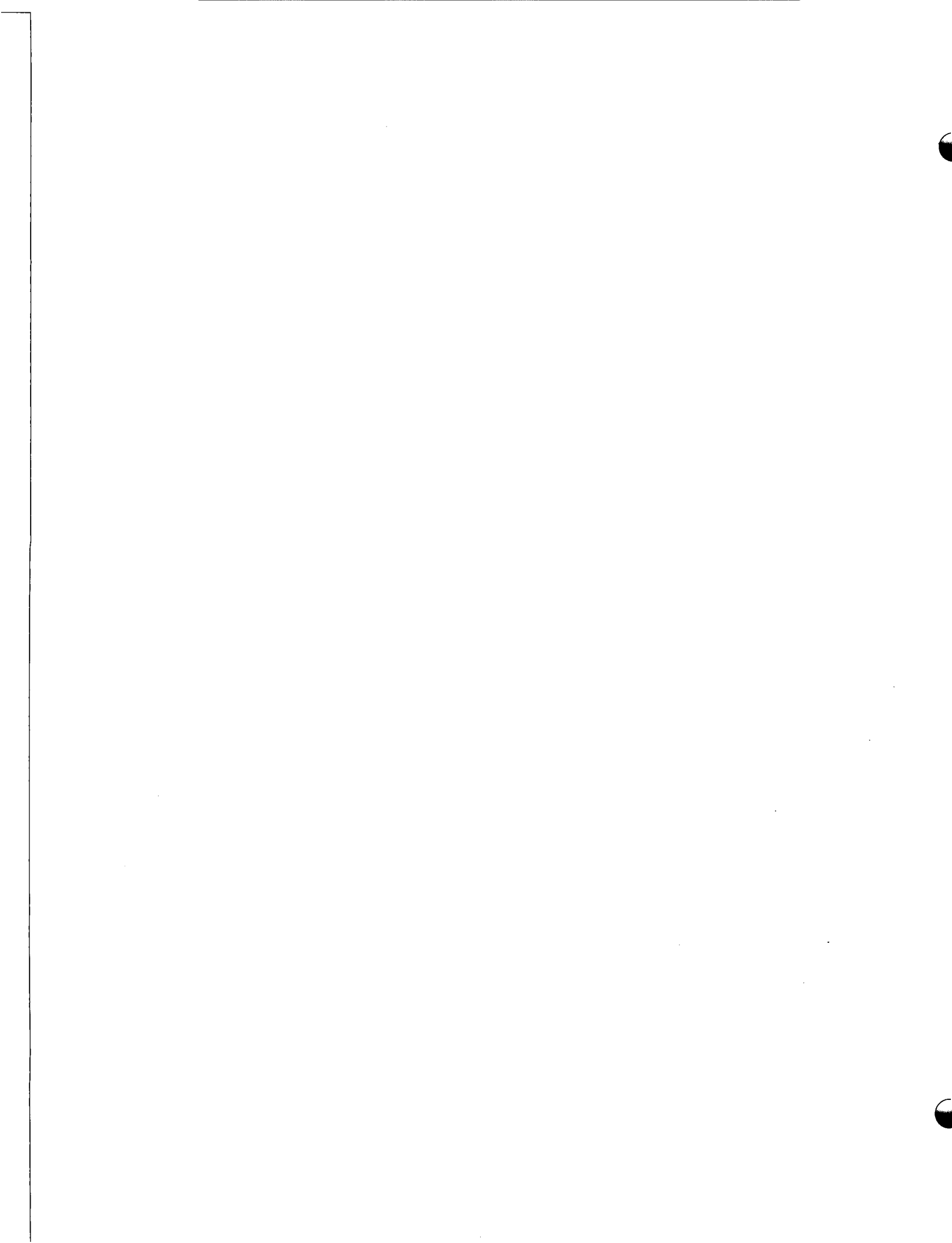
August 1978

Abstract

Simulation studies have recently been made of the Krafla Geothermal Field in Northern Iceland. The field is close to boiling in the formation at depths of 1800 meters and below. Two simulations were undertaken. The first studied radial flow, i.e., behavior around a production well. It was found that the relative permeability distribution of the liquid and vapor phase had very little effect on the general results. The simulation shows that while the well produced superheated steam after a few days of production, the superheated front moved only 1/10 the distance of the boiling front, which extended to a radial distance of over 200 meters after one-half year production. The second simulation investigated the two-zone system which is believed to exist in Krafla. This study simulated one well producing 50 kg/s from both zones for a period of 33 years. It showed that boiling in the formation begins near the production well and at the connection between the two zones. After 20 years, boiling takes place in the entire lower zone region with saturation (steam volume fraction) ranging from 0-30 percent. After 33 years, saturation increased to over 60 percent at the top of the lower zone, just under the caprock separating the two zones. Higher production rates will augment the spread of the saturation proportionately to the ratio of mass production.

*This work was supported by the Division of Geothermal Energy of the U.S. Department of Energy under Contract No. W-7405-ENG 48.

Rly



CONTENTS

Abstract	
Introduction.	1
Temperature and Pressure Measurements	7
Reservoir Modeling.	10
SHAFT78	13
Radial Flow	16
Two-Zone Simulation	44
Conclusion.	57
Acknowledgements.	59
Nomenclature.	60
References.	61

SIMULATION OF THE KRAFLA GEOTHERMAL FIELD

Introduction

Iceland is located on the plate boundary between the American and European tectonic plates which traverse the island from SW to NE. In Northern Iceland, the rift zone has a north-south direction. The structure of the neovolcanic zone in Northern Iceland is dominated by large swarms of faults and fissures most of which pass through the several central volcanoes where volcanic fissure eruptions, silicic rocks and high temperature geothermal fields are concentrated (Saemundsoon, 1974). Two central volcanoes, Krafla and Askja, have developed calderas. The swarms of faults and fissures are arranged in echelon subparallel to the north-south direction of the main zone. The northernmost parts of these fissure swarms are intersected in the area north of Axarfjordur by the Tjornes Fracture Zone which has an east-westerly direction (Fig. 1).

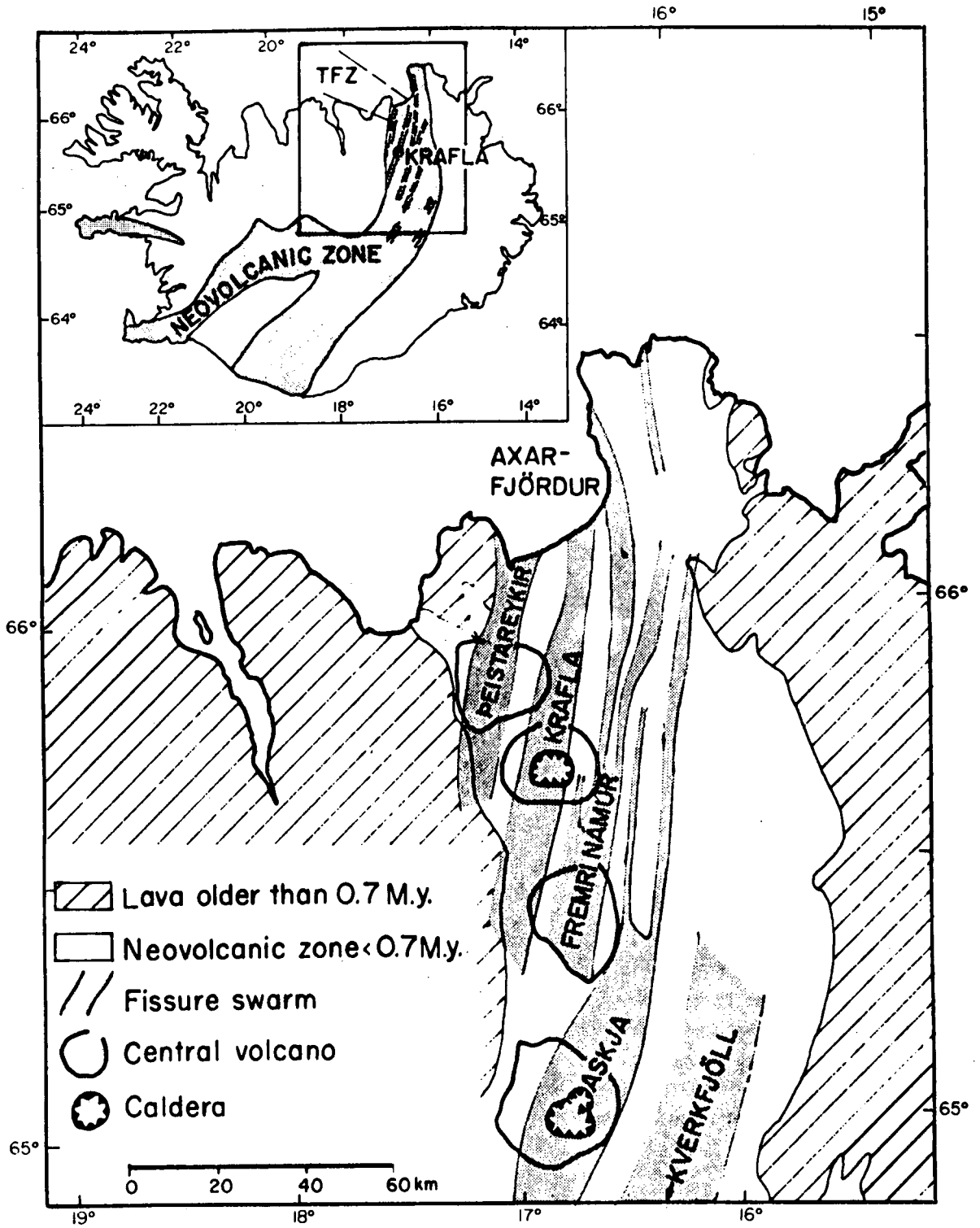
The Krafla caldera measures about 10km east-west and about 8km north-south. It was formed during the last interglacial period and has since been filled almost to the rim with volcanic material. The collapse of the caldera almost certainly followed the eruption of the dacitic welded tuff which is exposed around the caldera (Fig. 2). Field characteristics indicate that it is an airfall tuff which was blown mainly towards the NE from a source near the center of the caldera. A shield volcano at least 20km in diameter existed prior to the caldera formation. Remnants of this shield structure enclose the caldera on the east and west sides exposing lavas and braccias dipping outward at low angles. Dikes and eruptive fissures that trend parallel to the caldera ring faults are conspicuous around the caldera.

A high temperature geothermal area is located within the Krafla caldera.

Measurements taken from the eleven boreholes that have been drilled there indicate that the geothermal reservoir consists of two zones. The upper zone lies 500 - 1200 meters below the surface and has a temperature range of 210-220°C. The lower zone lies deeper, and its temperature ranges from 320-340°C. Indications show that the lower zone formation may be flashing, although it is not known whether this occurred before or after the opening of the boreholes. The lower zone fluid contains large amounts of carbon dioxide (CO₂), whereas the upper zone has much less carbon dioxide. The depth of the lower zone has not yet been determined, but it exceeds 2200 meters, the depth of deepest borehole drilled to date. A sectional geological drawing made from west to east based upon the borehole data published by the National Energy Authority of Iceland (1977) is shown in Fig. 3. The distance from the surface to the lower zone is shortest on the east side of the field with a 100 meter thick nonpermeable cap between the two zones; but on the west side the distance is 1600 - 1800 meters with a cap 500 meters in thickness separating the two zones. Non-condensable gas measurements indicate that the two zones connect east of the boreholes presently drilled, and that heat flows up from the lower zone to the surface near Hveragil, a fumarole on the west side of Mt. Krafla which is located 600-1200m east of the boreholes.

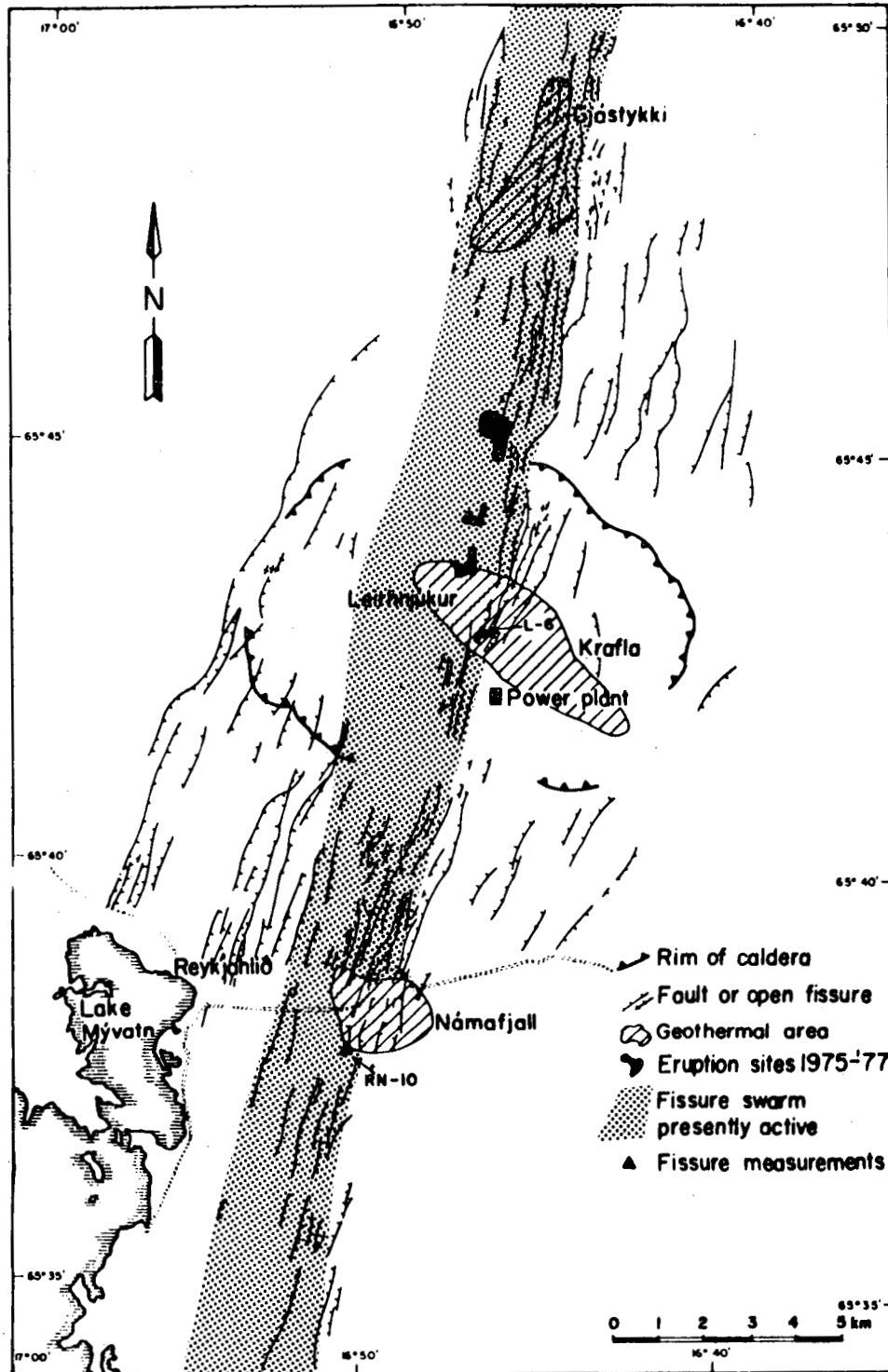
On December 20, 1975, an eruption occurred in Mt. Leirhnjúkur which resulted in spectacular rifting episodes still not completed by August, 1978. Intense earthquakes, widespread ground deformation, and magmatism are affecting an 80km long segment of the plate boundary (Bjornsson, et al., 1977 and 1978). The effect on the geothermal reservoir is difficult to determine, but the gas content of the lower zone has increased by as much as a factor of ten. There

are indications that magma flowing into a magma chamber 3-7 km from the surface has caused a steady uplift of 6-7 mm/day at its maximum near the center of the caldera. When the land has risen to a certain height an increase in the frequency of earthquakes has been observed followed by a sudden subsidence, over a period of a day or so, of approximately 10-100 cm in the center of the caldera. This has occurred eight times since the eruption of December, 1975, and was followed twice by short eruptions.



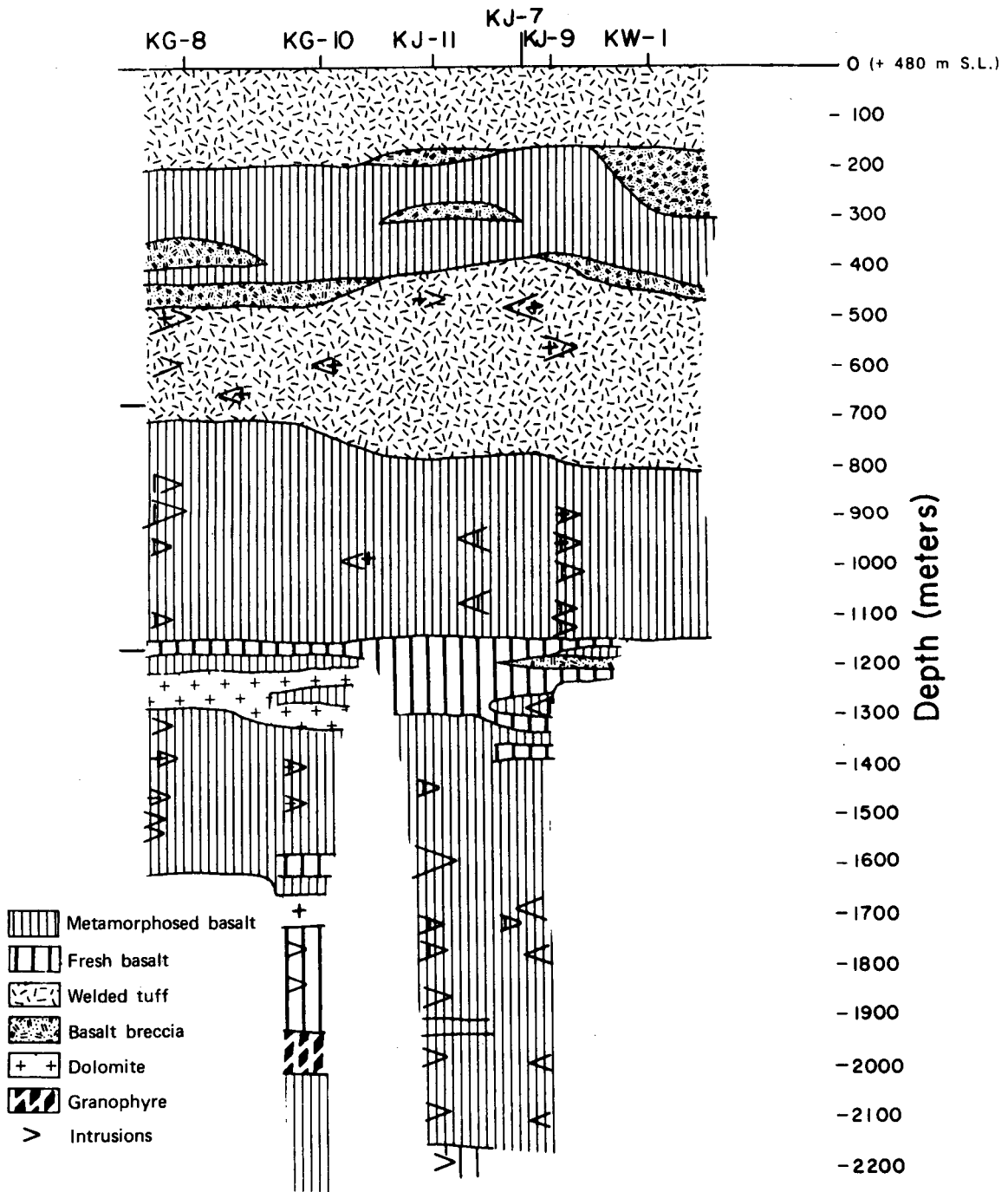
XBL 793-8932

Fig. 1. The spreading zone in North Iceland. The high-temperature geothermal fields and fissure swarms are named after the central volcano. Mapped by Kristian Saemundsson, (Bjornsson et al., 1978).



XBL 793-8931

Fig. 2. Outline geological map of the Krafla Caldera and associated fissure swarm. Mapped by Kristian Saemundsson (Bjornsson et al., 1978).



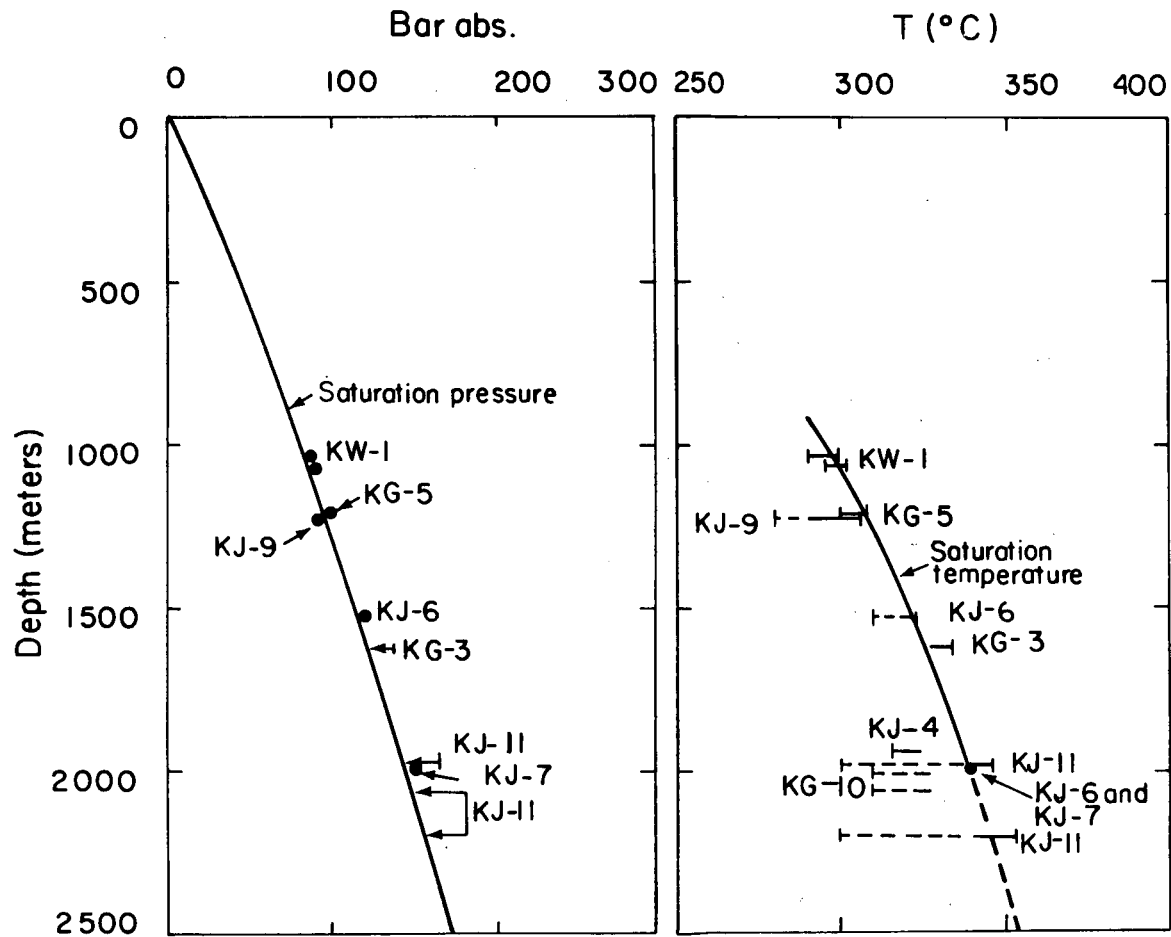
XBL 788-1474

Fig. 3. Sectional geological drawing of the Krafla geothermal field.

Temperature and Pressure Measurements

It is essential to ascertain the temperature and pressure of the geothermal reservoir before modeling can proceed. A summary of all the pressure and temperature measurements taken from the eleven boreholes in the Krafla geothermal field is shown in Figs. 4 and 5. Although the pressure is slightly higher than the saturation pressure, it can be assumed that because of the high concentration of CO₂ (3-5% by mass), the partial pressure of the gas in the reservoir is approximately 5-6 bar. The temperature in boreholes 6 and 7 has been more accurately determined than that in other boreholes since the temperature falls right on the saturation curve at the 2000 meter depth.

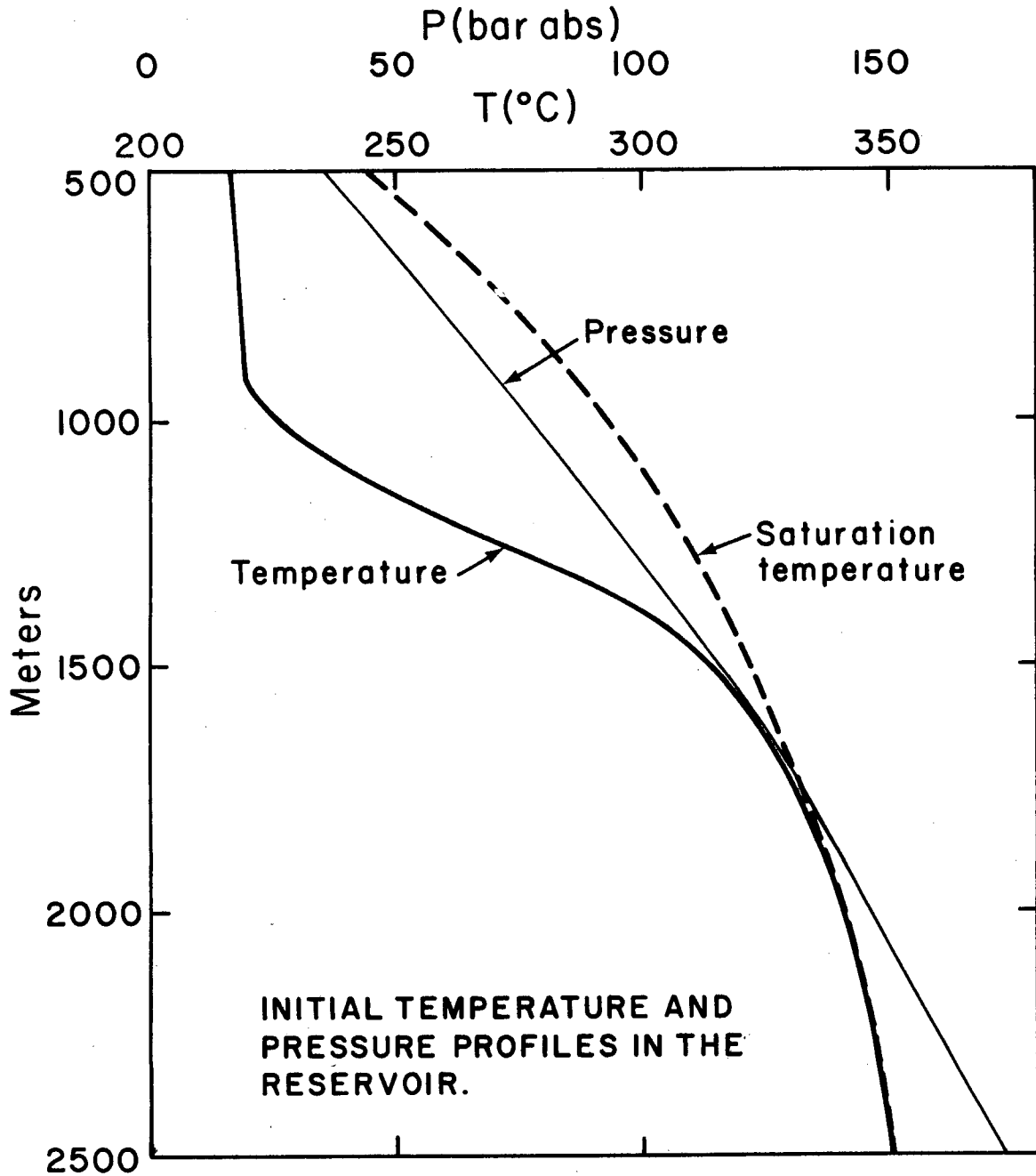
Figure 6 shows the pressure and temperature profiles used as the initial condition in the SHAFT78 computer simulation model. As indicated above, the temperature lies along the saturation temperature curve at depths of 2000 meters and below.



XBL-788-1475

Fig. 4. Pressure measurements in boreholes in Krafla.

Fig. 5. Temperature measurements in boreholes in Krafla.



XBL 788-1483

Fig. 6. Initial pressure and temperature profiles used in the simulation models.

Reservoir Modeling

There are indications that the Krafla geothermal field is located in the middle of the caldera, with the highest anomaly centered between Mt. Krafla and a fissure swarm which passes through the Leirhnjukur volcano. The maximum heat flow at the surface is near the fumarole Hveragil. Areal flow of deep water from south to north along the fissure swarms is estimated to be approximately 10^{-6} m/s. It is estimated that the Krafla geothermal field lies primarily in the southeast corner of the caldera and has an area of approximately 16-20km (Bjornsson, et al., 1977).

As mentioned above, there are substantial indications that the field is composed of two zones separated by a cap rock of extremely low permeability. This has made it difficult to interpolate permeability values for the two zones from the pumping tests (Sugurdsson and Stefansson, 1977) because most of the completed boreholes which penetrate both zones have perforations in their liners. It was possible to estimate permeability values for the two zones from the few boreholes which penetrate only the upper zone, and from other boreholes which have only a weak connection with the upper zone, yielding mostly from the lower zone. Values range from 10 - 60 md for the upper zone, and from 1 - 40 md for the lower zone. The values used for purposes of reservoir modeling are 30 md for the upper zone and 10 md for the lower zone.

The reservoir modeling can be divided into three studies:

1. Radial Flow: the effect of radial flow from the lower zone into a borehole.
2. Two-zone model: study of approximately 1/36 of the geothermal field by taking a 10° sector through the upper and lower zones.

3. Prediction of the behavior of the total geothermal field when producing 60MW and 120 MW electrical power.

Parts 1 and 2 have been completed, and the grid for part 3 has been generated; but the reservoir as a whole has not yet been simulated. Figure 7 shows the grid for the radial flow configuration, and Fig. 8 shows the grid arrangement for the two-zone modeling called KRAFLA 1. Figures 9 and 10 show three-dimensional drawings of one of the eight layers comprising the total geothermal area. This grid was generated by the grid generator computer program, OGRE (Weres and Schroeder, 1978). The smallest elements are concentrated around the 11 boreholes that have been drilled in Krafla.

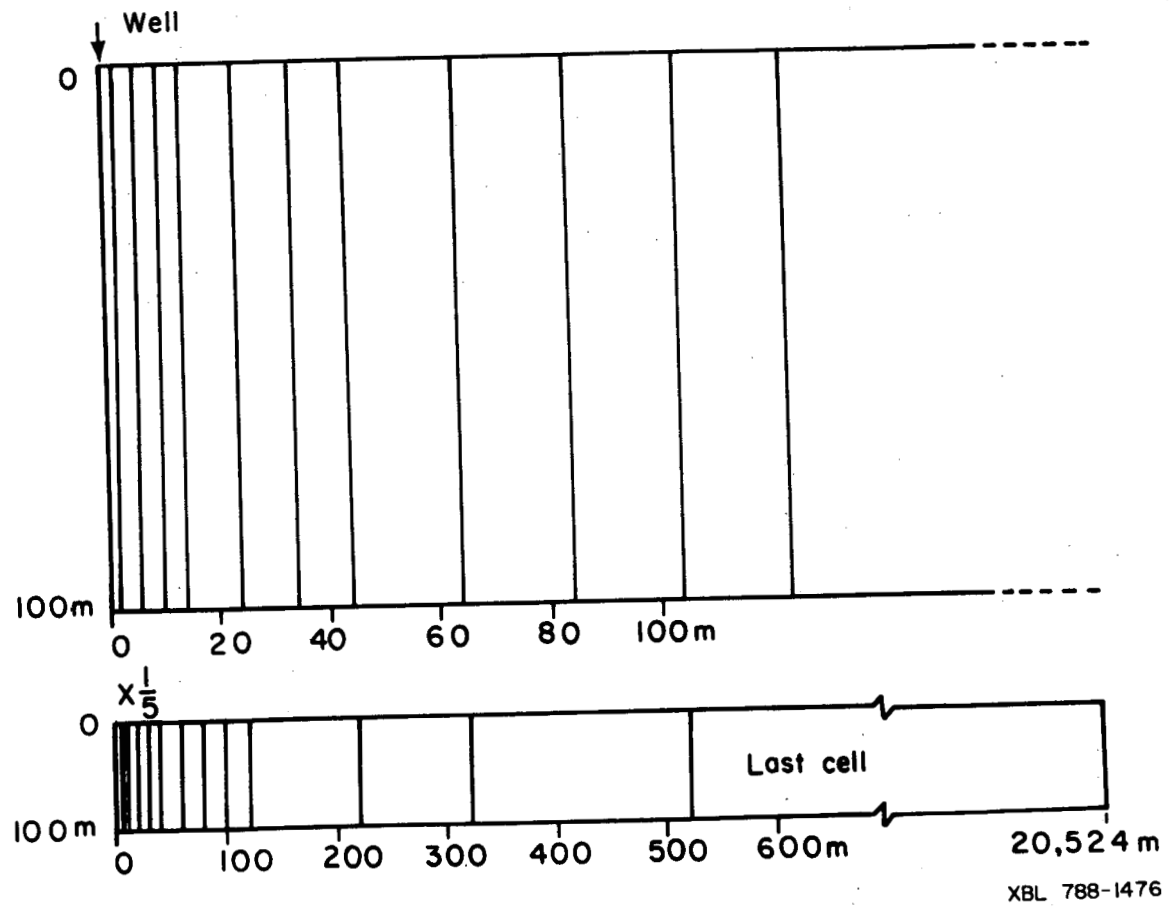
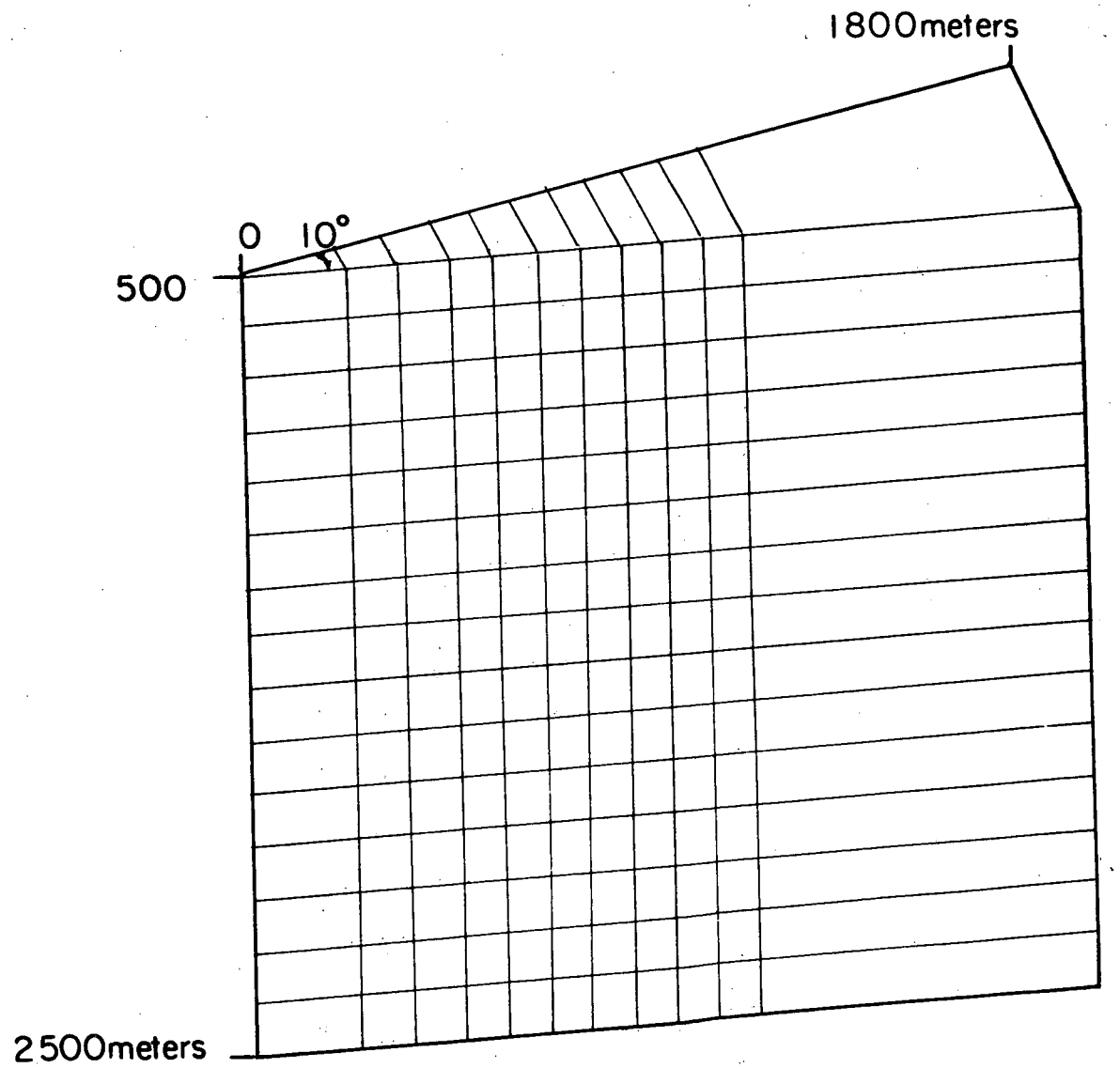


Fig. 7. Grid for radial flow simulation.

SHAFT78

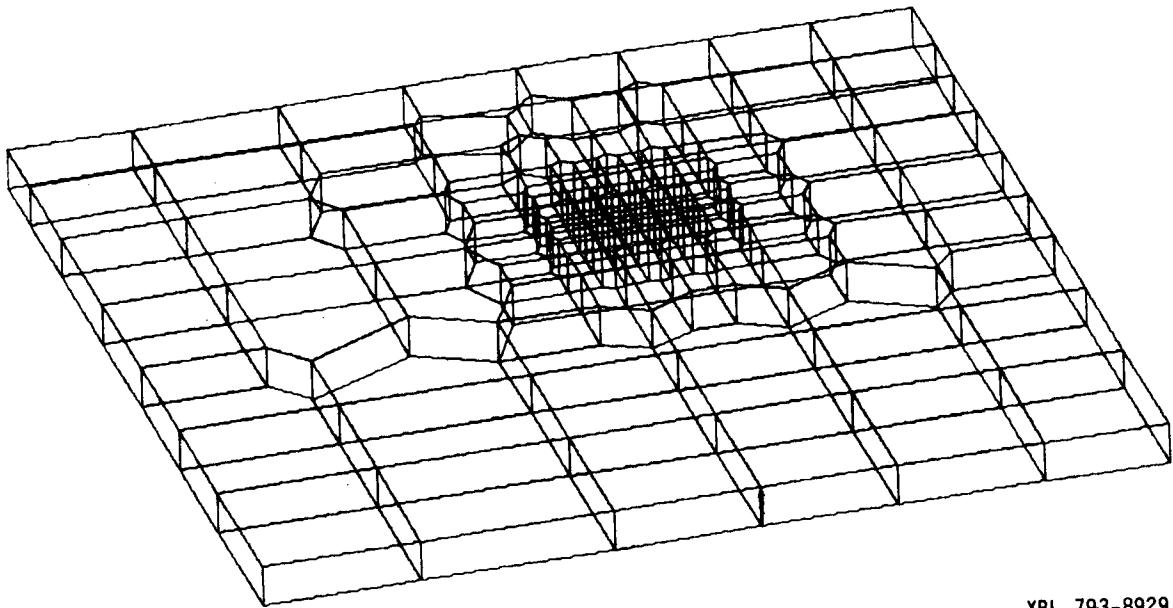
A computer program called SHAFT78 (Simultaneous Heat and Fluid Transport) has been developed at LBL. This program gives a numerical solution in three dimensions of the coupled equations for the conservation of mass and energy together with Darcy's flow equations for one-or two-phase fluid in porous media.

The SHAFT program has been under development for many years, and this year's SHAFT78 version has been extensively checked for accuracy against analytical and other numerical solutions in the two-phase region and in the transition from one-phase to two-phase flow (Pruess et al., 1978). The basic concept of SHAFT78 is to solve the governing equations in terms of two variables, fluid specific energy and density. This approach has a considerable advantage over the traditional method using temperature, pressure, and saturation; for fluid specific energy and density are always independent variables even in the two-phase region, whereas temperature and pressure are not. The description of the numerical solution procedure and the equation of state for water in terms of specific energy and density is given in Pruess et al., (1979).



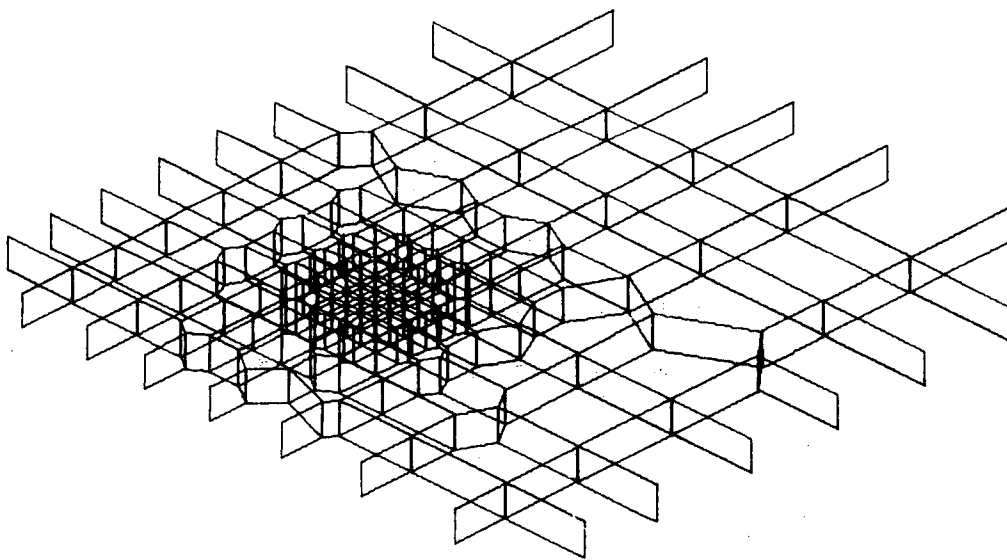
XBL 788-1477

Fig. 8. Grid for two-zone simulation.



XBL 793-8929

Fig. 9. Grid for simulation of Krafla geothermal field



XBL 793-8930

Fig. 10. Grid for simulation of Krafla geothermal field.

Radial Flow

In order to simulate a flow of water flashing in the formation near a borehole, the radial flow grid shown in Fig. 7 was generated; 1/64 of a full circle is taken into consideration. The layer has a constant thickness of 100m; the permeability is uniform and equal to 10md; the porosity of the rock is 0.1; the rock density is equal to 2650 kg/m³; and the specific heat of the rock is assumed constant at 950 J/kg°C. A constant mass flow was withdrawn from the corner element at a rate of 0.25 kg/s, which corresponds to 16 kg/s taken from the total area surrounding the borehole. The pressure and temperature are initially assumed uniform at 140 bar and 332°C, respectively. This corresponds to a layer located approximately 1900 meters deep at Krafla.

In order to calculate two-phase fluid flow, it is common to separate the Darcy equations into two equations for vapor and liquid. Darcy's law for each phase is given by:

$$F_v = \frac{\rho_v k R_v}{\mu_v} (\nabla \bar{P} - \rho_v \bar{g}) \quad (1)$$

$$F_l = \frac{\rho_l k R_l}{\mu_l} (\nabla \bar{P} - \rho_l \bar{g}) \quad (2)$$

where R_v and R_l are the relative permeabilities for vapor and liquid.

Very little data is available for the relative permeability of water. Recent measurements of the relative permeability of water have been done at Stanford by Chen (1976, 1978). Corey (1954) has derived equations for the relative permeability of gas and water known as the Corey equations.

For water:

$$R_{\lambda} = \begin{cases} \left(\frac{r-S}{r}\right)^4 & \text{for } S \geq r \\ 0 & \text{for } S > r \end{cases}$$

For steam:

$$R_v = \begin{cases} \frac{S^3(2r-S)}{r^4} & \text{for } S \leq r \\ 1 & \text{for } S < r \end{cases}$$

Fig. 11 shows the relative permeability distribution which is used as a default value by SHAFT (curves 1) and two relative permeability sets for Corey's constants equal to $r = 0.35$ and 0.75 , respectively.

These three cases, designated cases 1, 2, and 3, respectively, were used in the radial flow simulation. For Case 1, 3 x 250 energy cycles were computed. For Cases 2 and 3, 2 x 250 energy cycles were computed. On the average, 8-9 flow cycles were computed for each energy cycle. Table 1 shows the different cases computed.

Table 1. Cases Computed

	0-250 cycles	250-500 cycles	500-750 cycles
Case 1	Case 1.1	Case 1.2	Case 1.3
Case 2	Case 2.1	Case 2.2	-----
Case 3	Case 3.1	Case 3.2	-----

A computer plotting routine, PLOTZ, has been prepared which can plot pressure, temperature, saturation, and energy density-distribution for a specified number of energy cycles. These variables have been plotted at intervals of 25 cycles, which corresponds to 10 curves on each drawing. Figures 12 - 30 show the distribution of variables for all three cases. Table 2 gives the times at which these distributions were plotted. (These times are also indicated on the figures.)

Figures 12, 13, and 14 show the energy distribution for Cases 1.1, 1.2 and 1.3 respectively. Starting from a value of 1515 kJ/kg at the well-head, the energy reaches a maximum value of 2565 kJ/kg from about 100 hours for Case 3, to 250 hours for Case 1. Afterwards it remains practically constant except that the energy distribution becomes more dispersed as time increases. The depletion of specific internal energy is greater for Case 2 than for Case 1, while Case 3 shows the largest depletion.

Steam saturation (flashing) distribution in the formation is shown in Figs. 15-17 for the three cases during the first 250 energy cycles. The first element becomes fully saturated by steam in 250 hrs, 48 hrs, and 40 hrs. respectively for Cases 1.1, 2.1, and 3.1. The first 10 meters from the center of the borehole reached complete steam saturation in 480 hrs, 483 hrs, and 600 hrs (Case 3.2), respectively, for the three cases. This indicates that although Case 3 reaches complete steam saturation first, the spreading of the steam saturation front is similar for all the cases. The limit of the steam front ($S=0$) extended 44m from the center of the borehole in about the same time for all cases, 460 hrs.

Figures 18-20 show the pressure drop in the formation for the first 250 cycles. It appears that the drop in pressure during the first 250 cycles

TABLE 2. Times for Functions Plotted

CYCLES	CASE 1.1	CASE 2.1	CASE 3.1	CASE 1.2	CASE 2.2	CASE 3.2	CASE 1.3
25	1.5 hrs	1.4 hrs	1.6 hrs	30.0 days	29.5 days	26.4 days	93.7 days
50	3 hrs	2.8 hrs	2.6 hrs	(720 hrs) 35.0 days	33.6 days	30.1 days	101.6 days
75	16.4 hrs	15.5 hrs	14.3 hrs	40.7 days	37.1 days	34.0 days	109.8 days
100	50.2 hrs	48.2 hrs	39.8 hrs	46.5 days	41.5 days	38.1 days	118.5 days
125	93.7 hrs	108.3 hrs	86.2 hrs	52.6 days	46.7 days	42.4 days	127.6 days
150	146.2 hrs	180.2 hrs	161.0 hrs	58.9 days	52.3 days	46.8 days	137.2 days
175	248.9 hrs	273.4 hrs	298.6 hrs	65.5 days	57.8 days	51.5 days	147.4 days
200	348.7 hrs	372.4 hrs	383.1 hrs	72.4 days	63.4 days	56.4 days	157.8 days
225	461.0 hrs	473.8 hrs	468.6 hrs	79.6 days	68.6 days	61.5 days	186.8 days
250	585.0 hrs	583.2 hrs	522.2 hrs	87.3 days	74.7 days	66.8 days	180.4 days

determines the time steps taken by the computer program, for in all three cases the pressure dropped to 100 bar at the element containing the borehole, or $\nabla P=40$ bars. The pressure therefore falls fastest for Case 3 largely because the mobility of steam is only about 0.4 of the mobility of water for the existing conditions. The pressure distribution is otherwise very similar for the three cases, and it is interesting to observe that no abrupt change in the pressure gradient can be seen over the flashing front, as is commonly believed.

Figures 21 and 22 show the temperature distribution of the fluid and the formation for cases 1.1 and 1.3. As a result of flashing and the drop in pressure, the equilibrium temperature of the fluid and the rock formations must also drop. The temperature drop after 250 energy cycles is 17°C for Case 1, and 13°C for Case 3, but the temperature depletion in a corresponding time interval is greater for Case 3, as can also be seen from the energy distribution in Figs. 15-17.

Because the distribution curves are similar for all three cases, it is superfluous to show each of them in the following discussion. Only typical distributions will be presented.

Figure 23 shows the energy distribution for Case 3.2. Please note that the increase in the radial distance is now twice as large as in the previous cases. The kink near the top of the curve occurs at the point where steam changes from superheated to saturated steam. The internal energy increase for the entire 250 energy cycles of 60 days is 15 kJ/kg at the first element, giving a final specific energy of 2580 kJ/kg.

Figures 24 and 25 show the steam saturation for Cases 1.2 and 3.2. The steam front and liquid saturation move at about same speed for the two cases (note the difference in time for each set of curves), but the shape

of the boiling zone is slightly different. This can be explained by the difference in the relative permeabilities of the two cases. A comparison of all three cases will be shown later for a corresponding time interval.

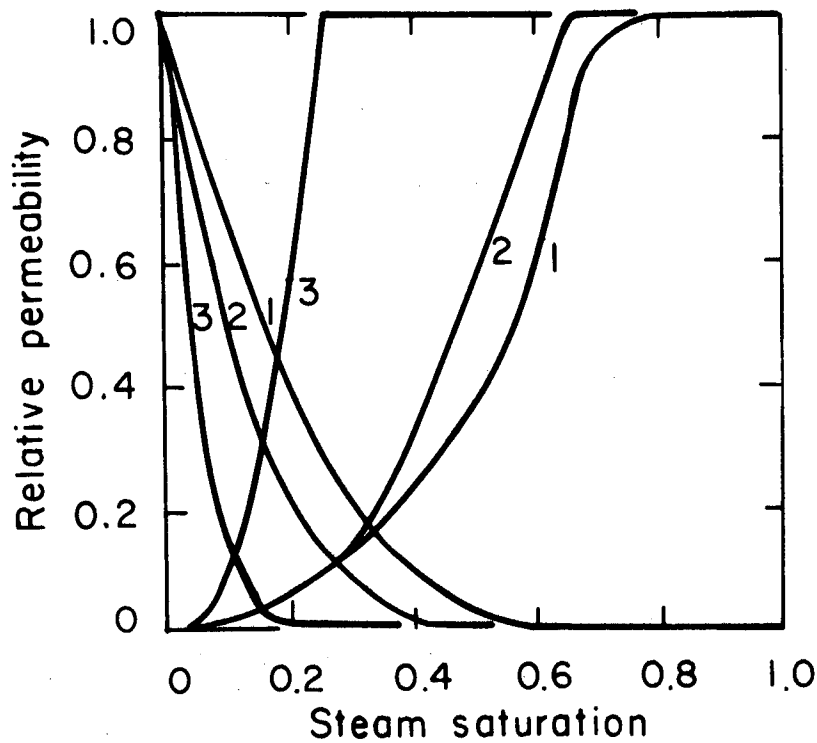
Figures 26 and 27 show the pressure depletion for Cases 1.2 and 3.2. Although the figures show a larger total pressure drop for Case 1.2 than for Case 3.2, the total pressure drop for Case 3.2 is in fact 7% higher for a corresponding elapsed-time from the beginning of the drawdown. The total pressure drop has decreased from $\Delta P=47.0$ bar at the end of Case 1.2 compared to $\Delta P=40.0$ bar at the beginning. Figure 28 shows the temperature depletion for Case 3.2. The temperature of the fluid and the rock formation continues to fall during the drawdown, yielding $\Delta T=5^{\circ}\text{C}$ throughout the time period considered, but $\Delta T=18^{\circ}\text{C}$ from the beginning of the drawdown.

Since the general behavior of the drawdown was similar for the three relative permeability values throughout the first 70-90 days, similar behavior can be assumed over longer time periods. Therefore, only Case 1 was used in simulating a longer drawdown period. It is interesting to observe how small an effect the relative permeability distribution has on the general behavior of the flashing zone and the pressure drawdown. Figures 29 and 30 show the flashing zone and pressure drawdown for up to one-half year of continuous mass production at a rate of 16kg/s.

Figures 31 and 32 sum up the results of this study by comparing steam saturation and pressure drawdown for radial flow in the three different cases considered after 46.7 days of continuous mass production. The corresponding values for Case 1.3 after 158 days are also given. The maximum difference in pressure at any location for the three cases is 3 bar, and

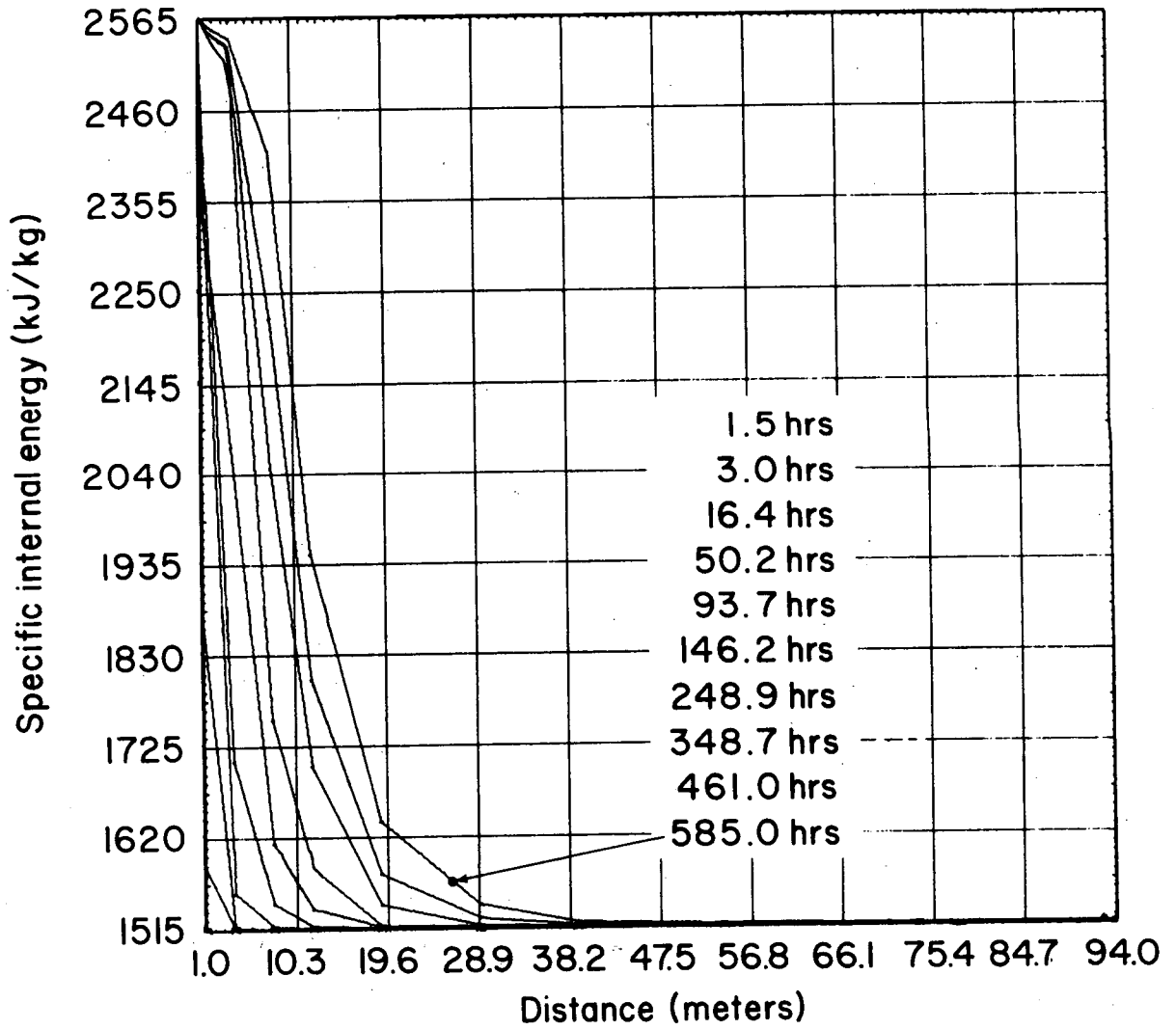
the maximum difference in saturation is 0.07. In both instances, this corresponds to 7% of the maximum difference. For Cases 1 and 3, which represent the extremes of relative permeability for which we tested, the superheated steam region and the flashing zone are identical, although the locations of saturation less than 0.5 differ slightly. If the two figures are compared, it can be seen that most of the pressure drop occurs across the superheated steam region and flashing zone for both time intervals considered. After 46.7 days, the pressure drop over the pure steam zone extending radially 15 meters from the center of the borehole is $\Delta P=26$ bar. The pressure drop over the flashing zone which extends outwards 15 to 100 meters is $\Delta P=13$ bar, and at the outer limit of the flashing zone the pressure is 7 bar below the initial pressure in the reservoir.

- 1 Relative permeability (Chen, H.K., 1976,1978)
- 2 Corey's equation with $S_{wi} + S_{gc} = 0.35$
- 3 Corey's equation with $S_{wi} + S_{gc} = 0.75$



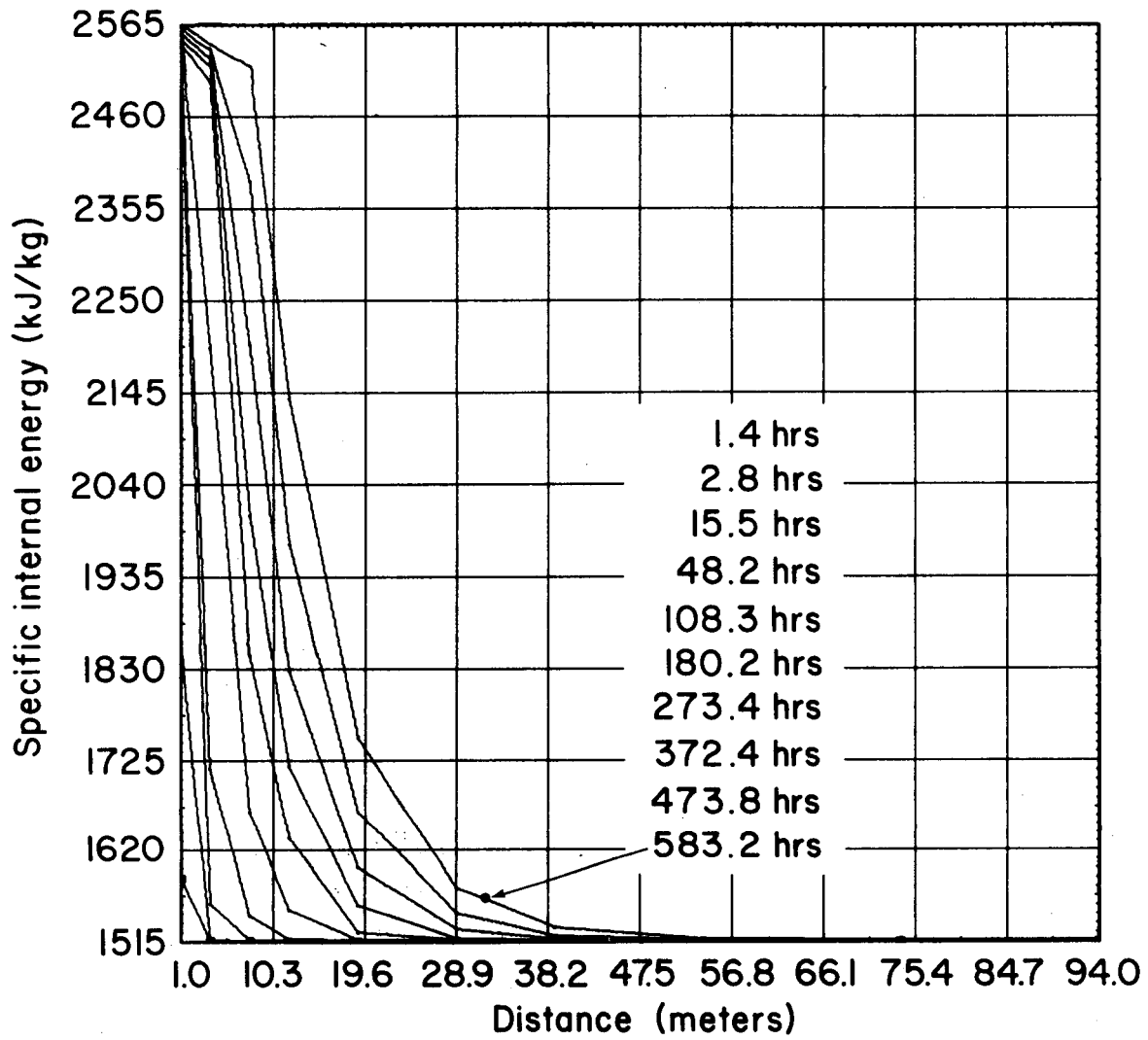
XBL 788-1473

Fig. 11. Relative permeability curves for the three cases studied.



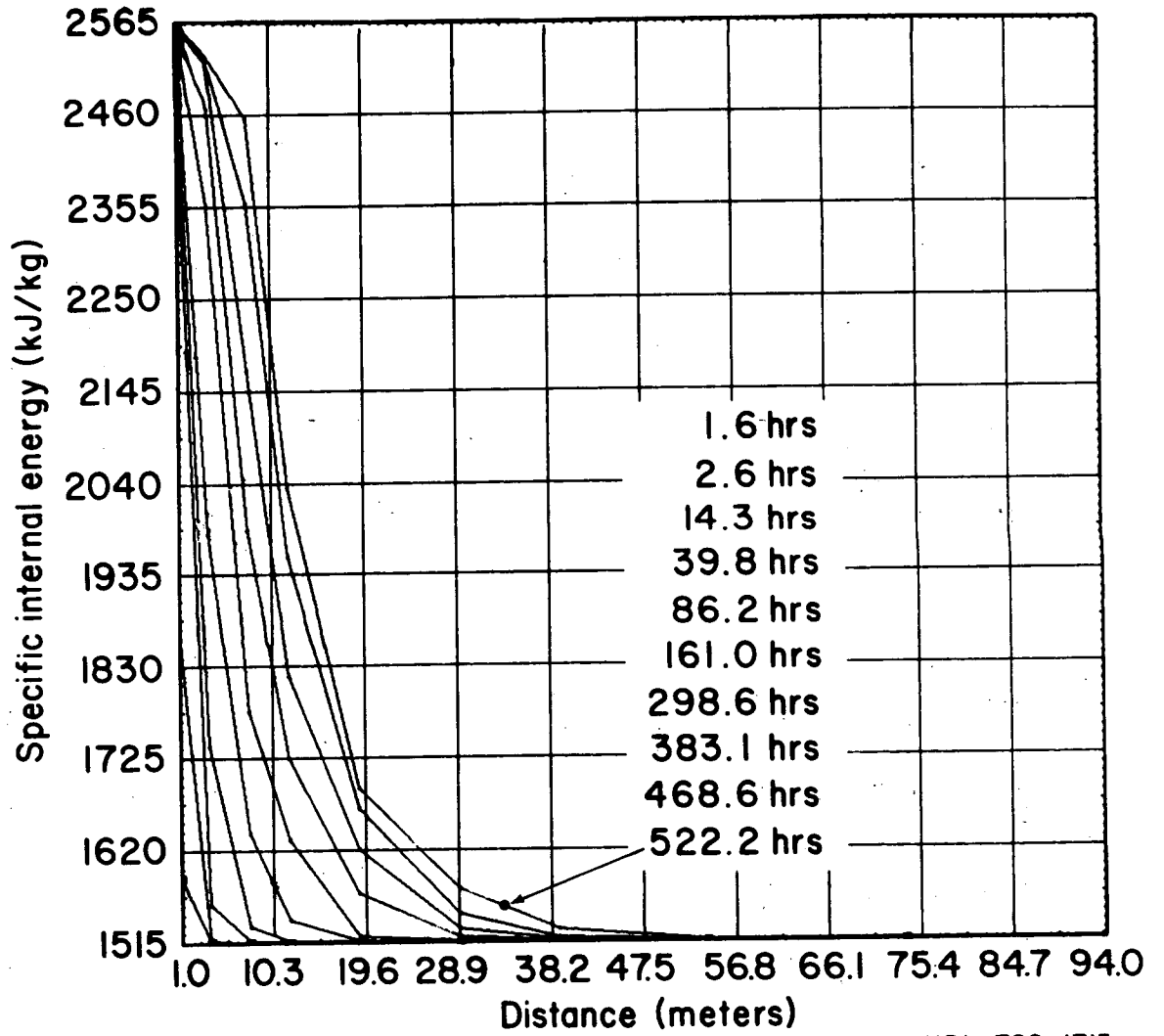
XBL 789-1713

Fig. 12. Internal energy distribution for radial flow, Case 1.1.



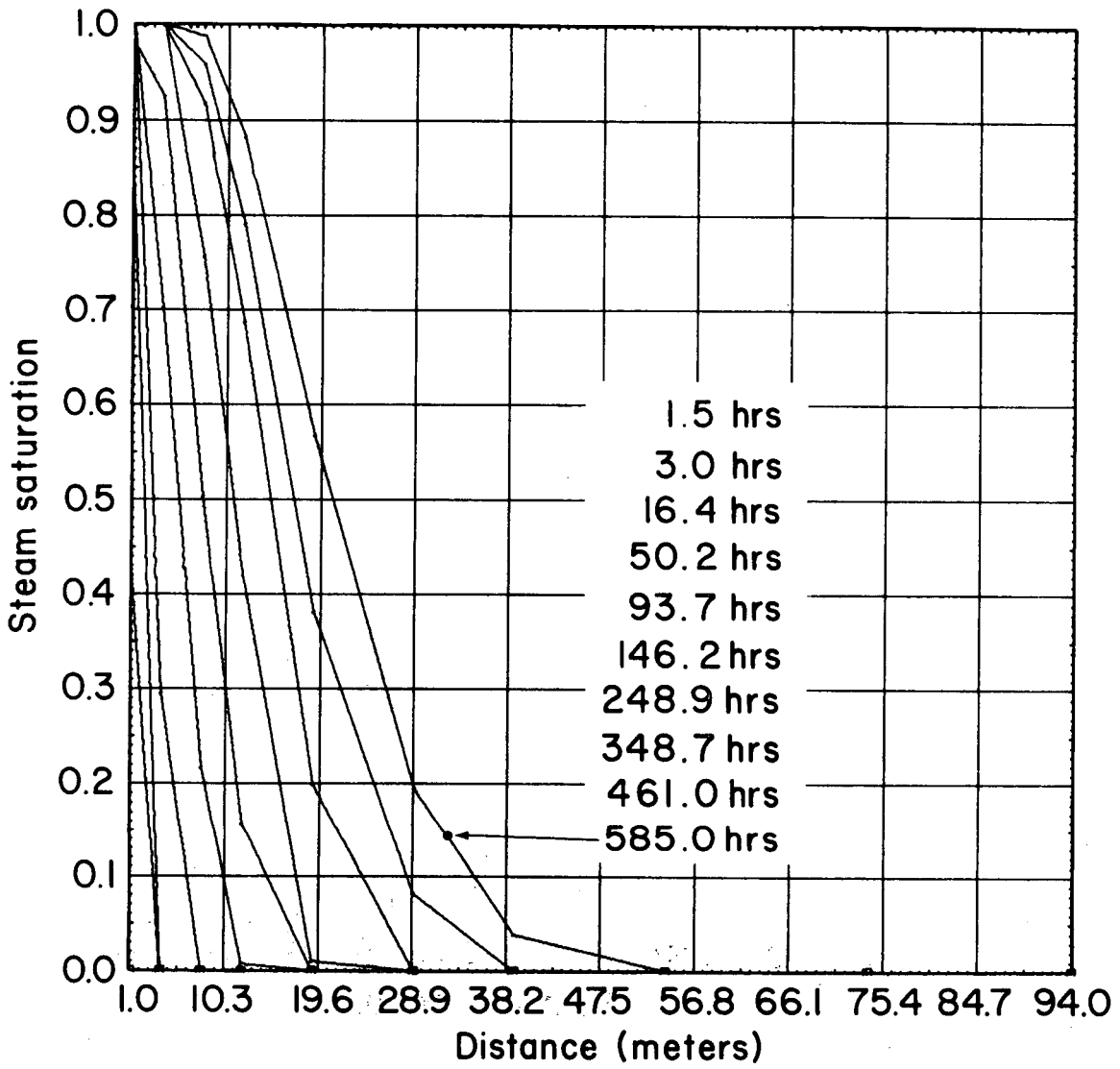
XBL 789-1714

Fig. 13. Internal energy distribution for radial flow, Case 2.1.



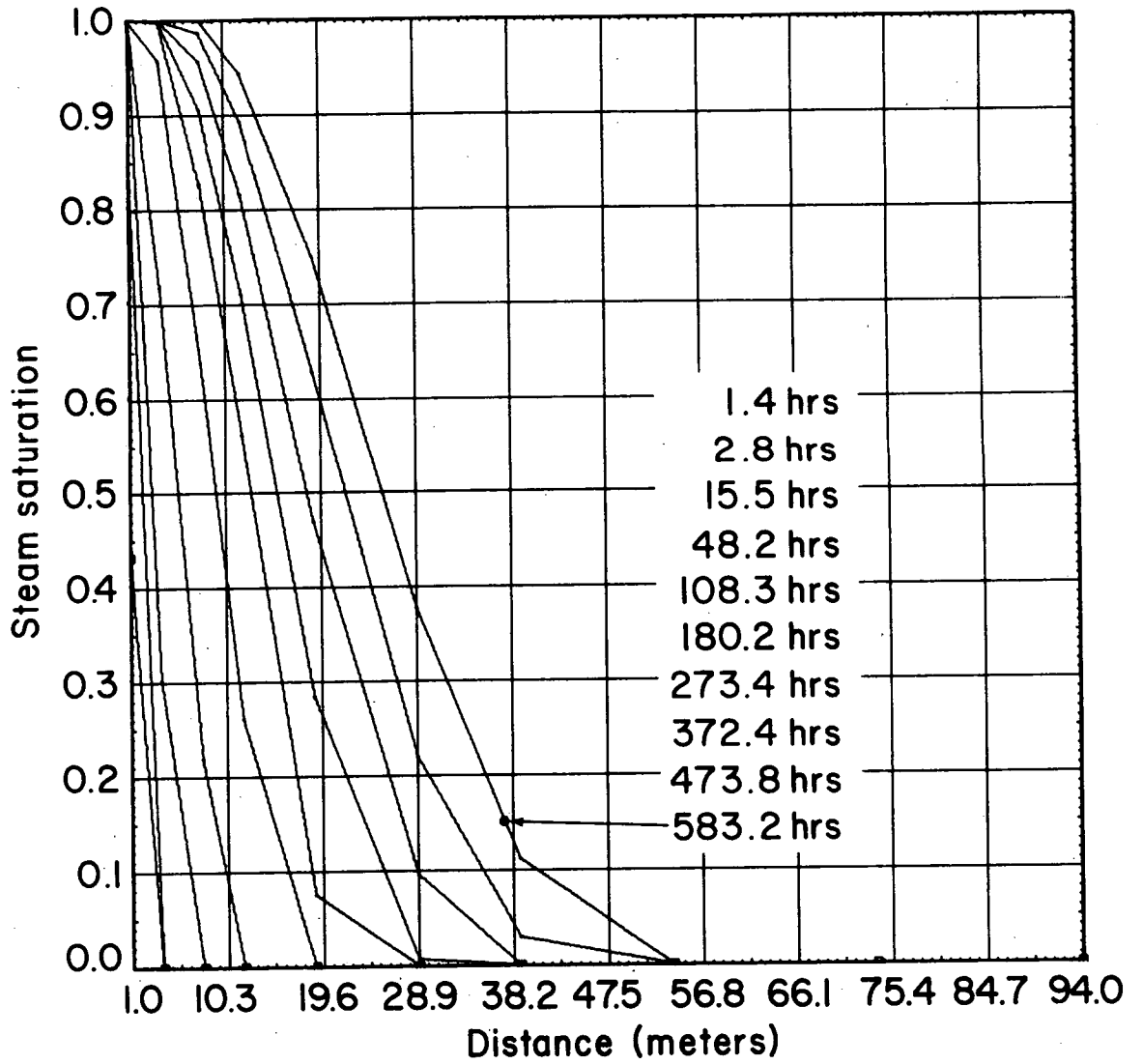
XBL 789-1715

Fig. 14. Internal energy distribution for radial flow, Case 3.1.



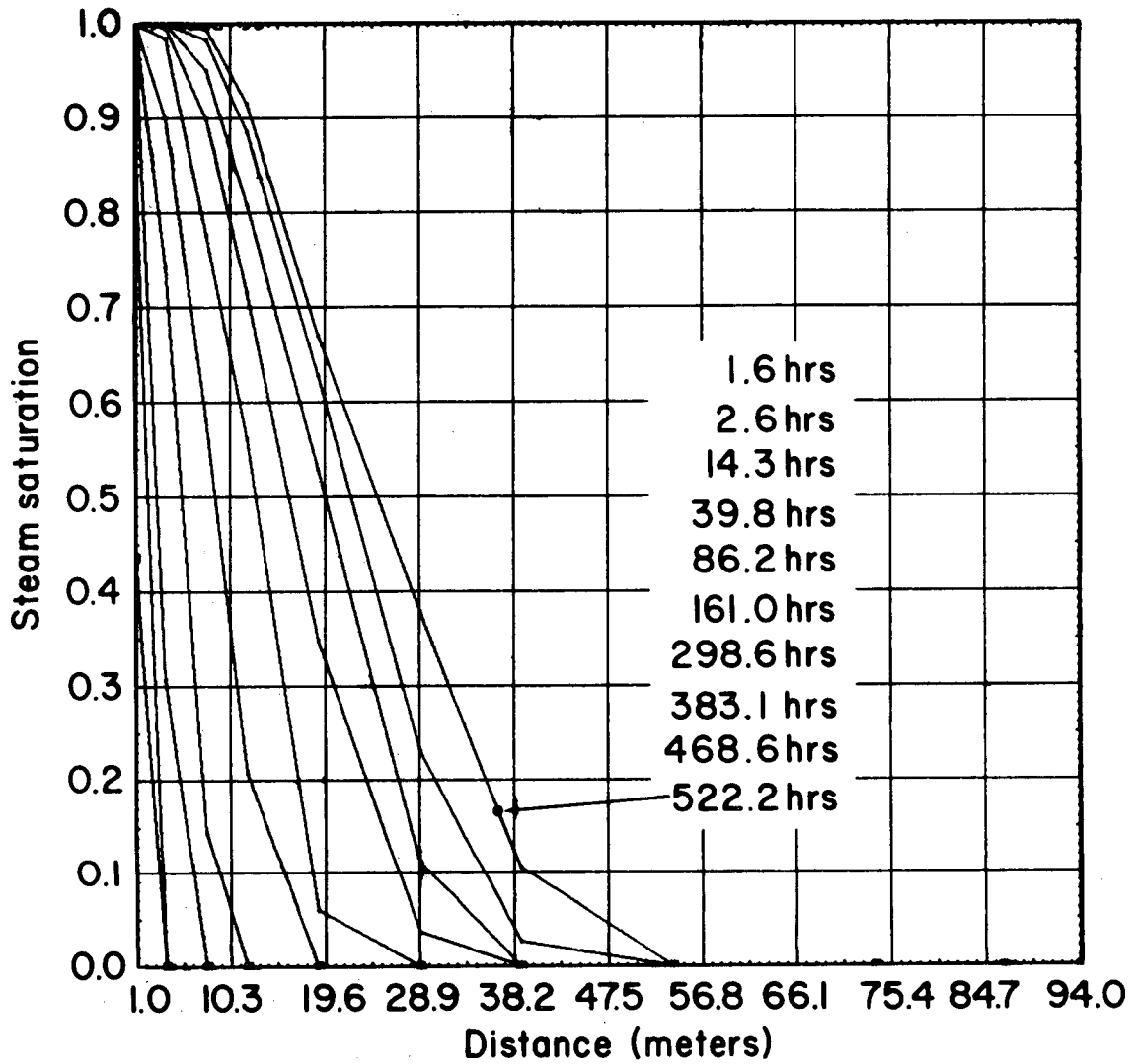
XBL 789-1716

Fig. 15. Steam saturation for radial flow, Case 1.1.



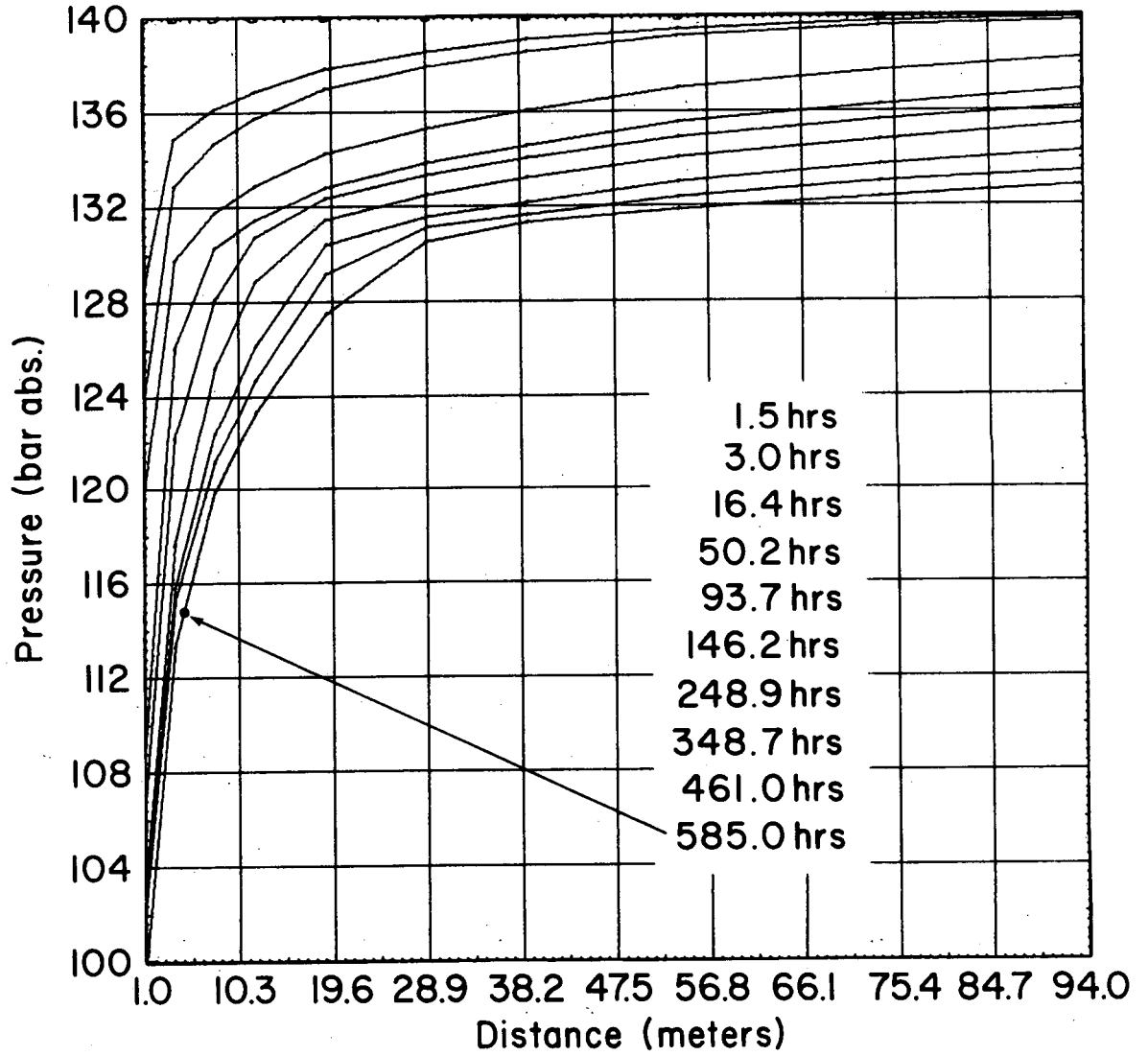
XBL 789-1717

Fig. 16. Steam saturation for radial flow, Case 2.1.



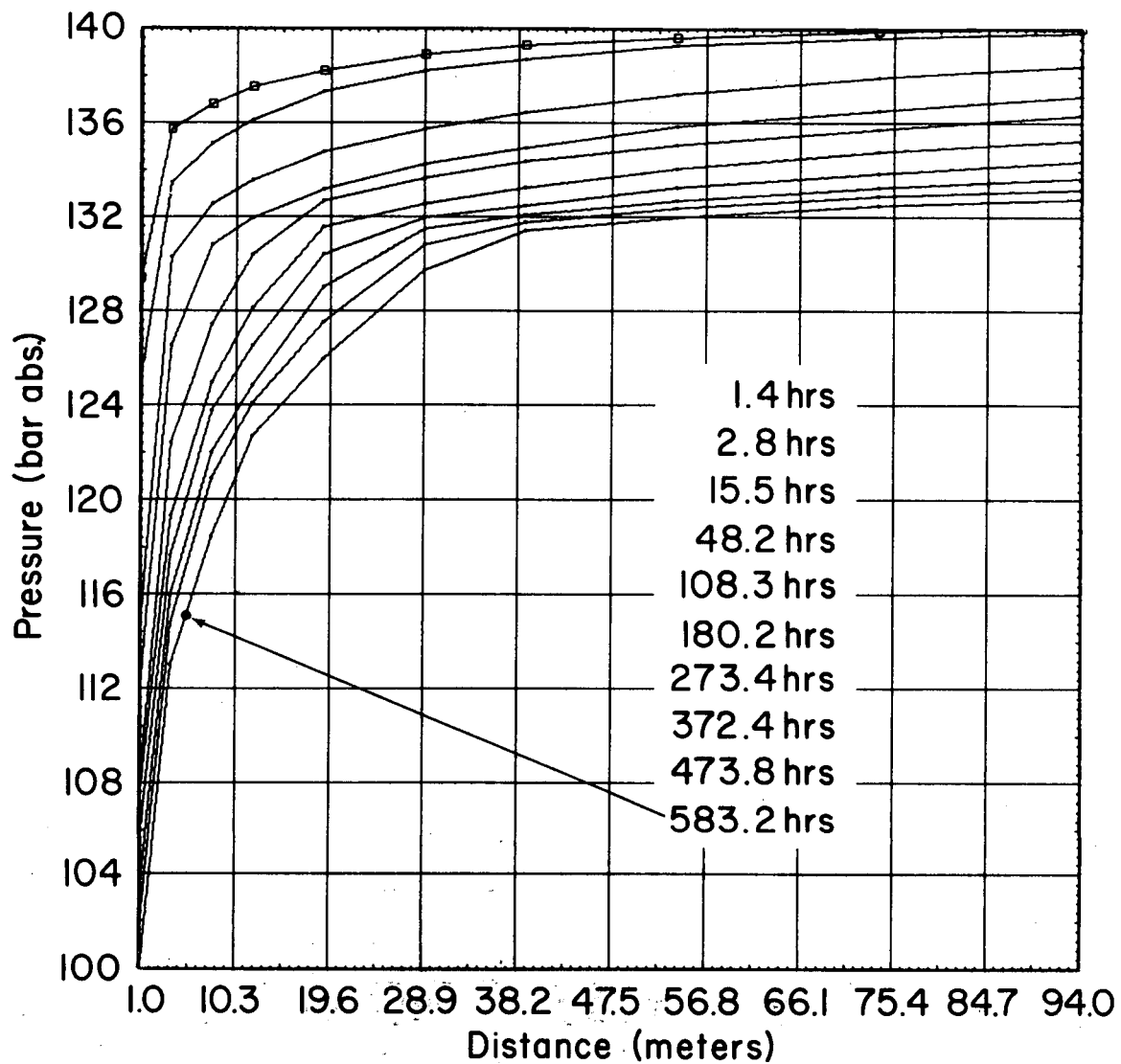
XBL 789-1718

Fig. 17. Steam saturation for radial flow, Case 3.1.



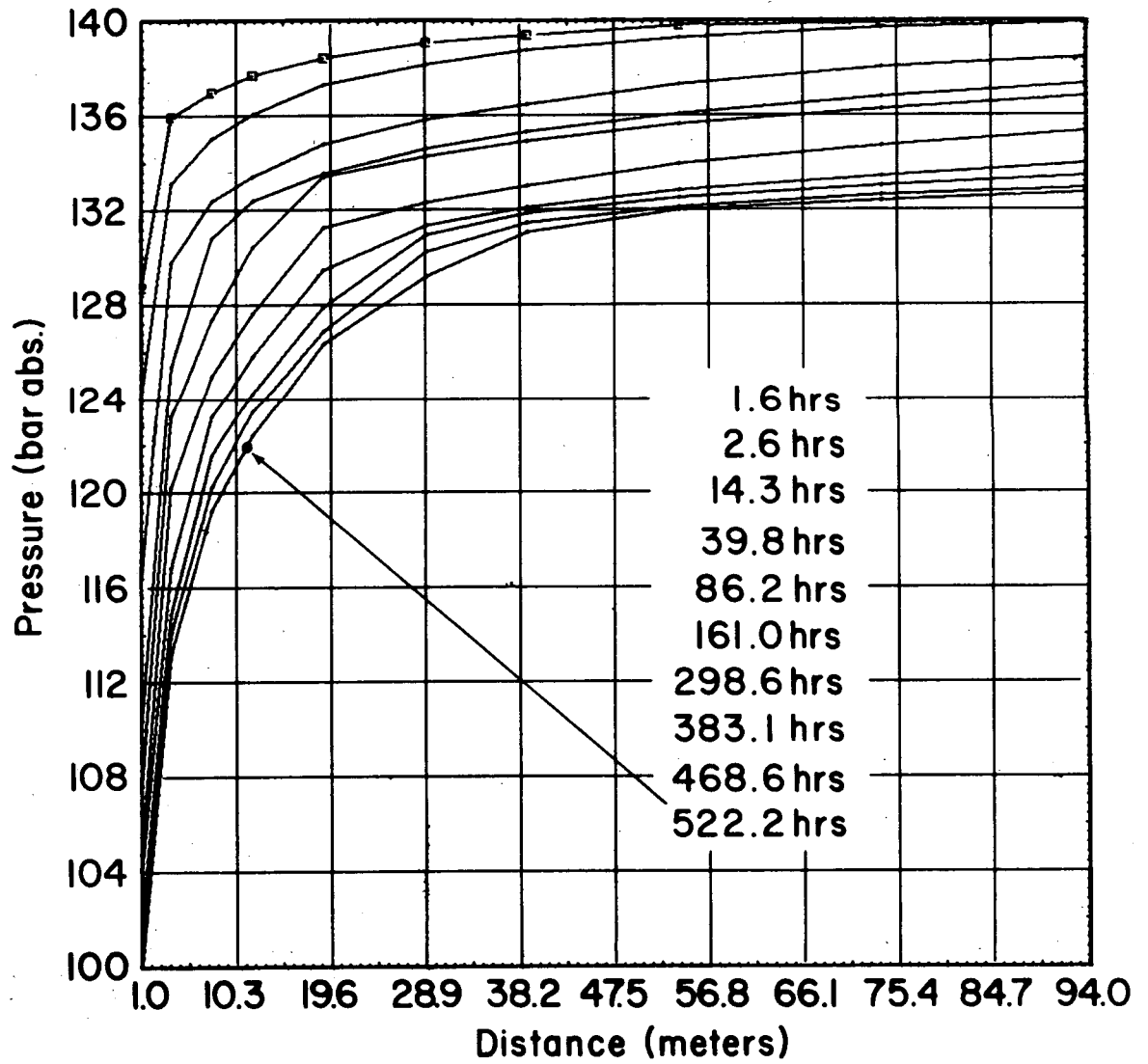
XBL 789-1719

Fig. 18. Pressure drawdown for radial flow, Case 1.1.



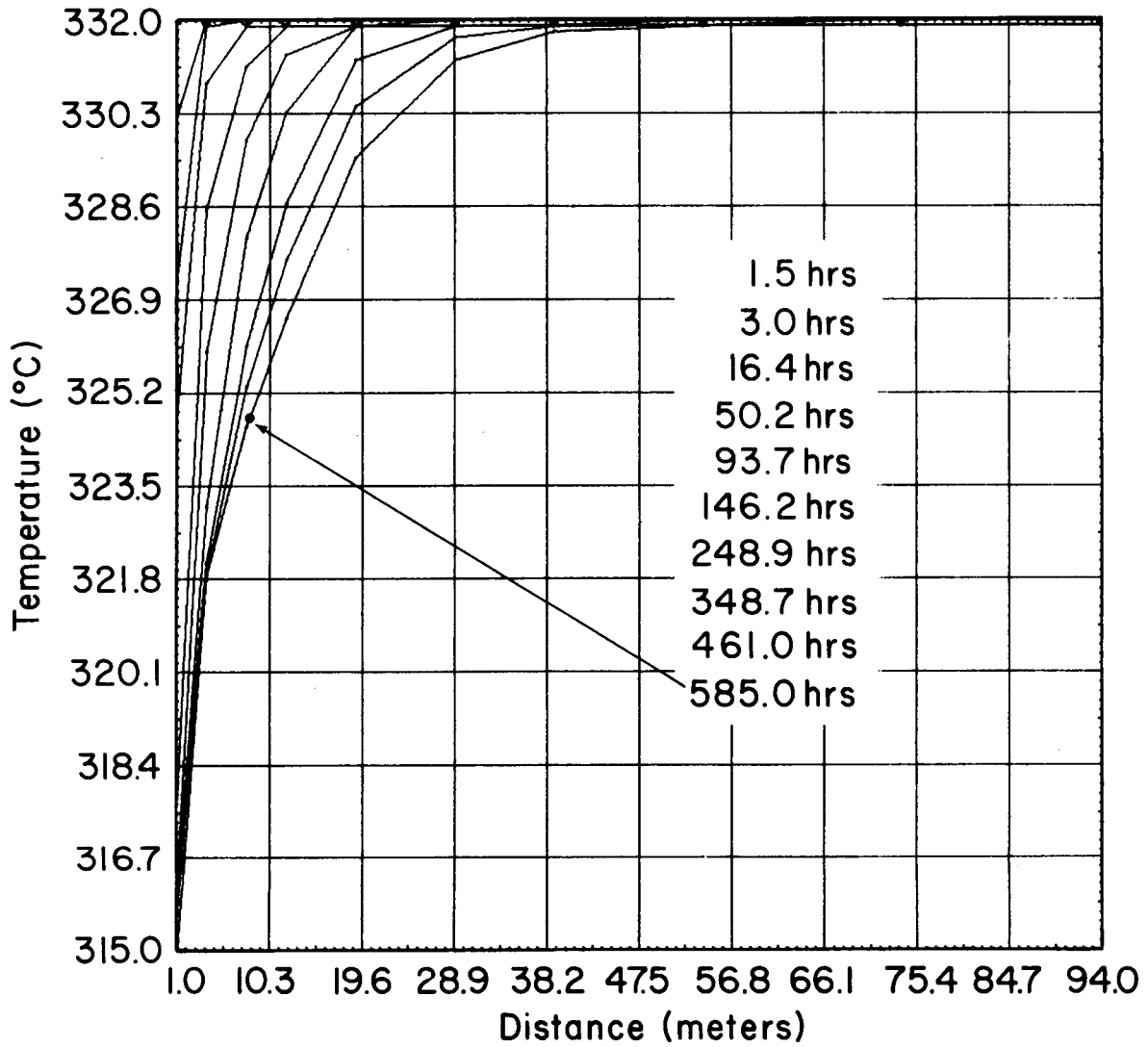
XBL 789-1720

Fig. 19. Pressure drawdown for radial flow, Case 2.1.



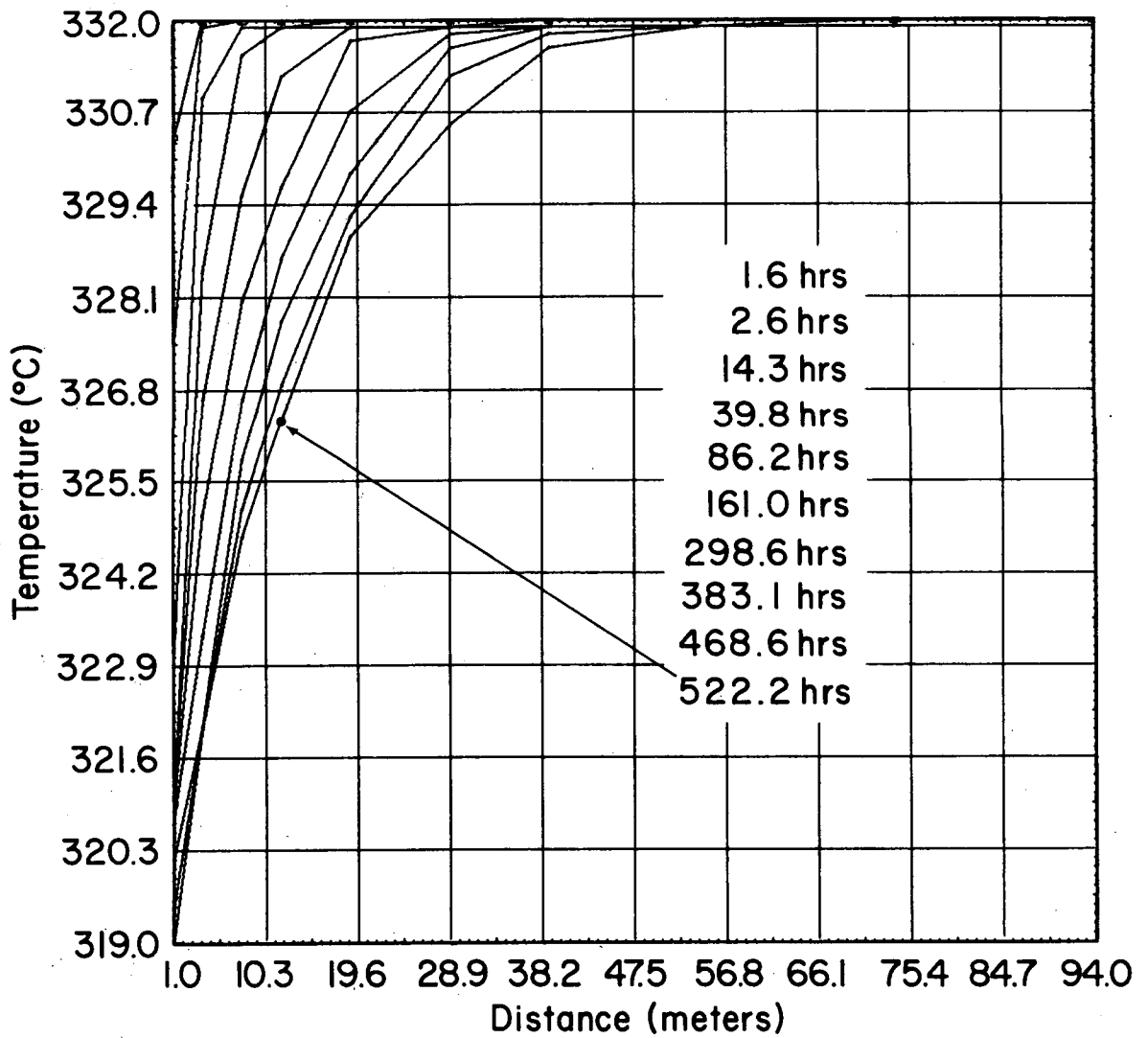
XBL 789-1721

Fig. 20. Pressure drawdown for radial flow, Case 3.1.



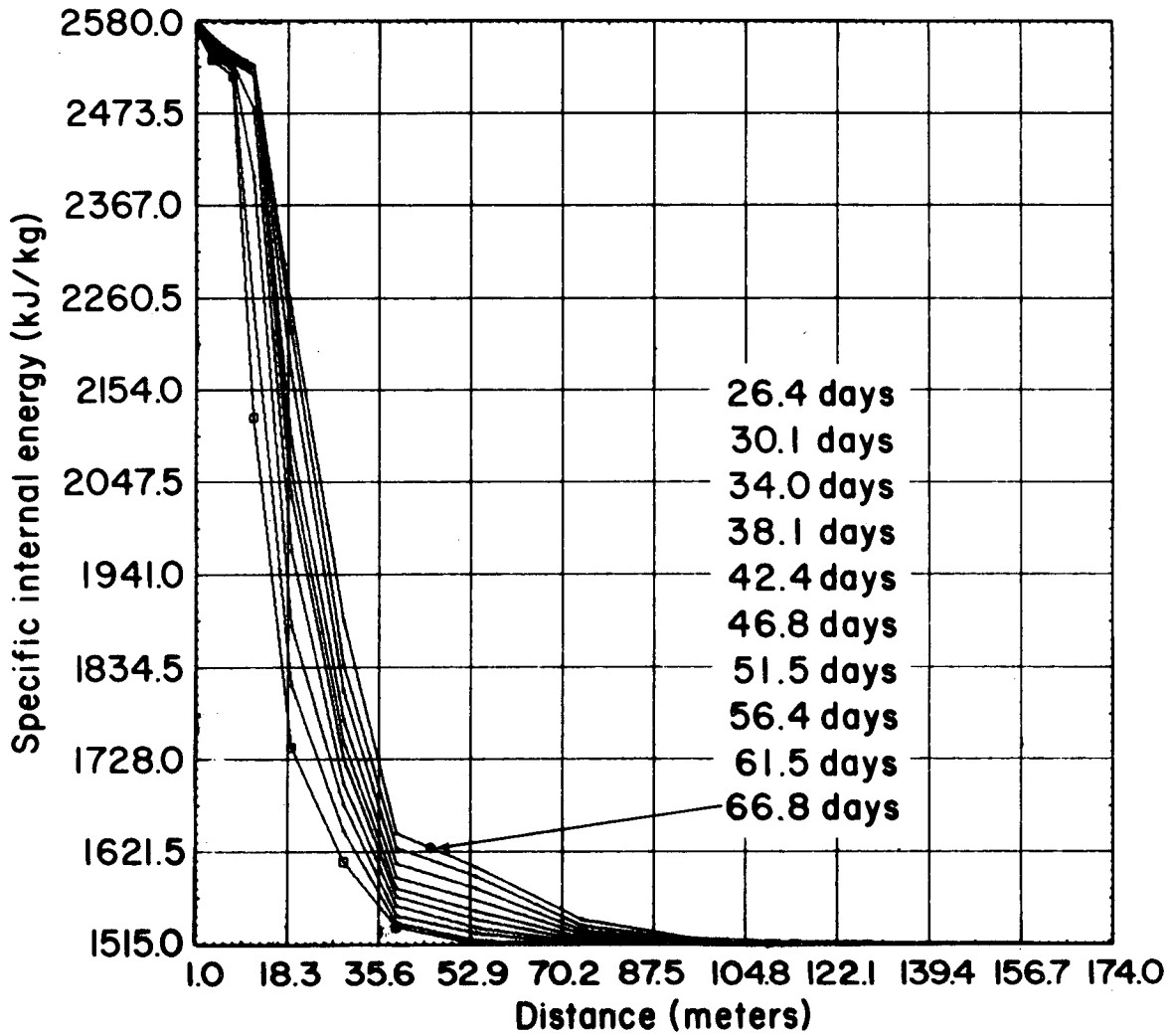
XBL 789-1722

Fig. 21. Temperature depletion for radial flow, Case 1.1.



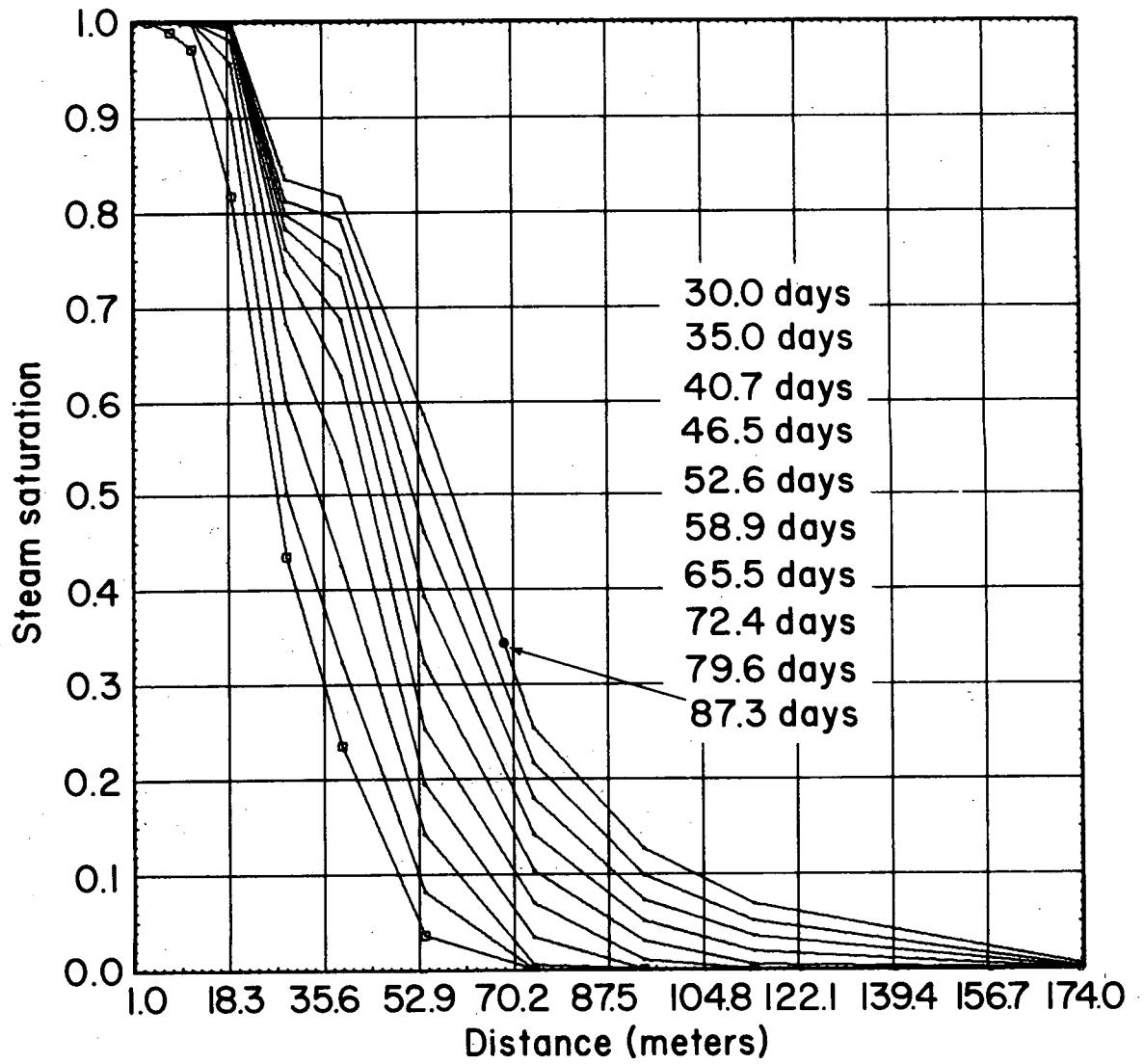
XBL 789-1723

Fig. 22. Temperature depletion for radial flow, Case 3.1.



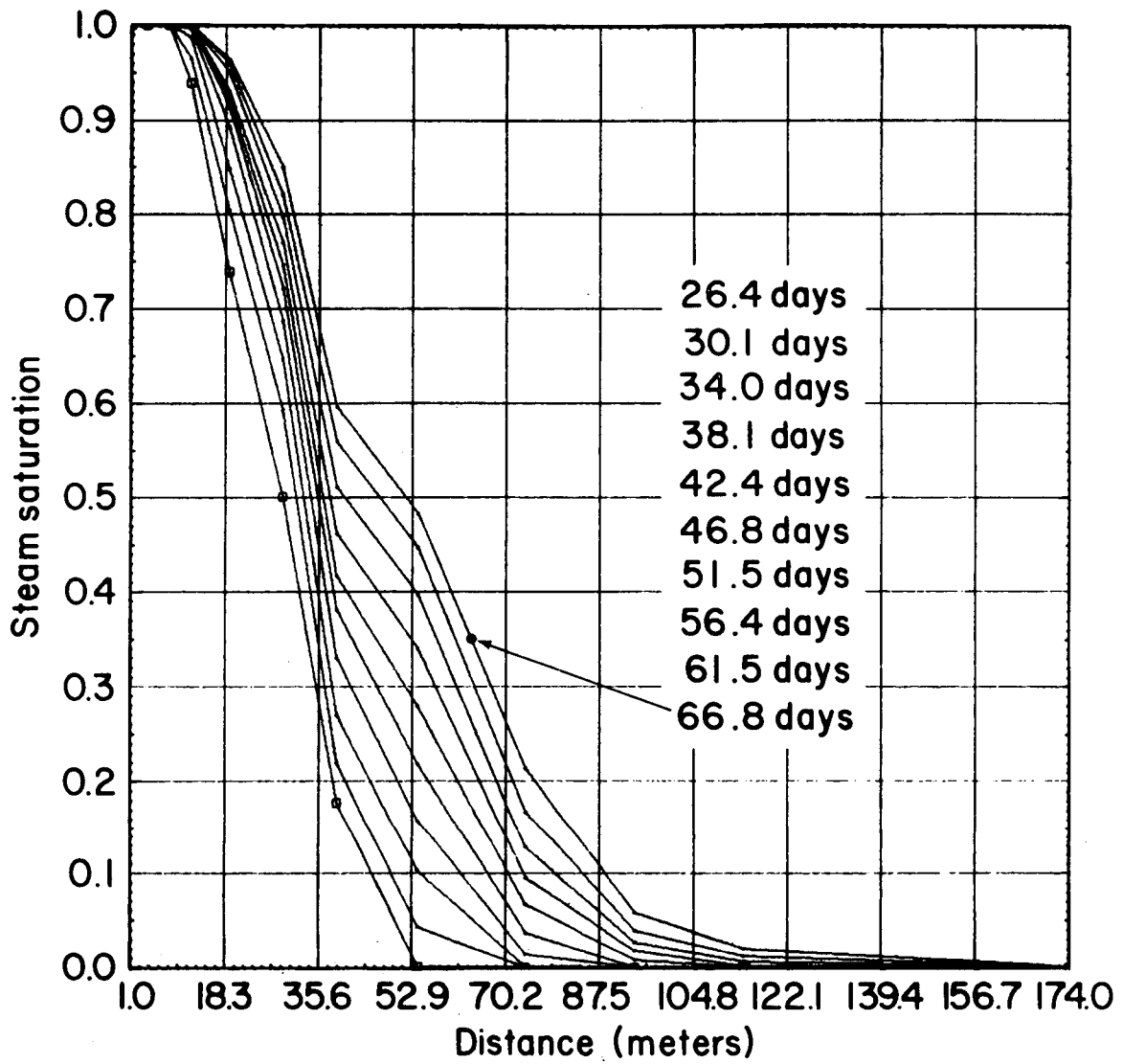
XBL 789-1724

Fig. 23. Internal energy distribution for radial flow, Case 3.2.



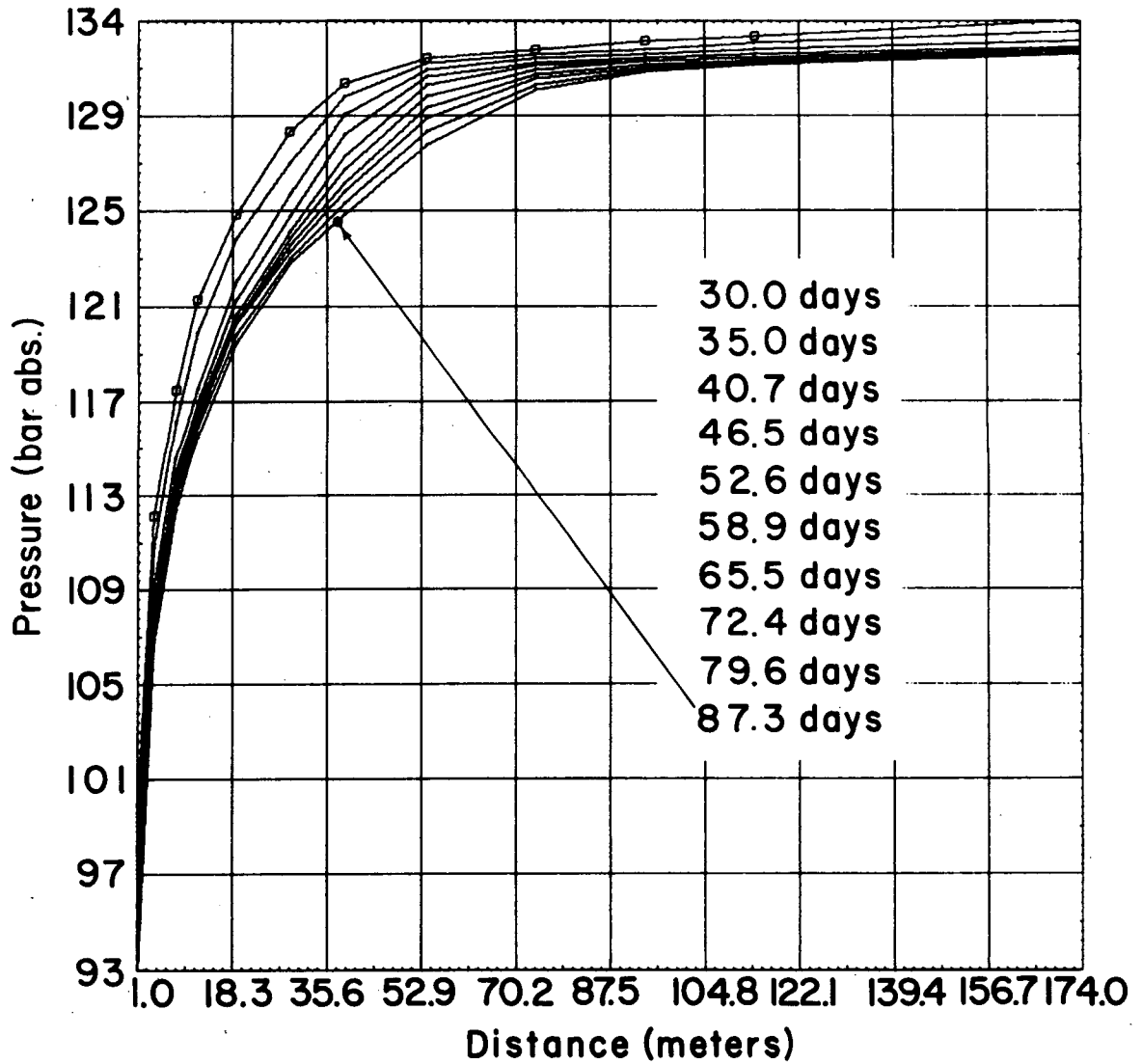
XBL 789-1725

Fig. 24. Steam saturation for radial flow, Case 1.2.



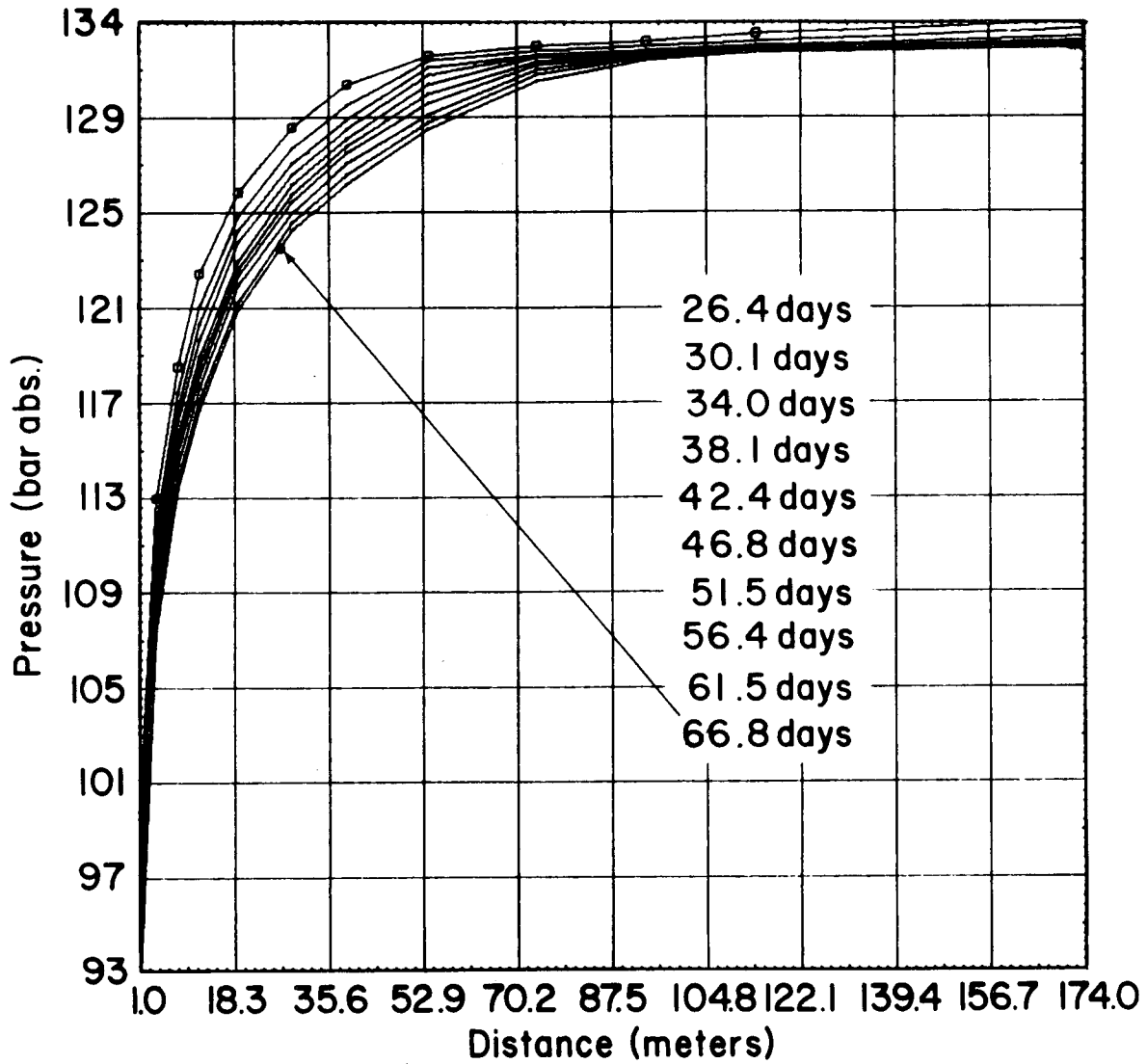
XBL 789-1726

Fig. 25. Steam saturation for radial flow, Case 3.2.



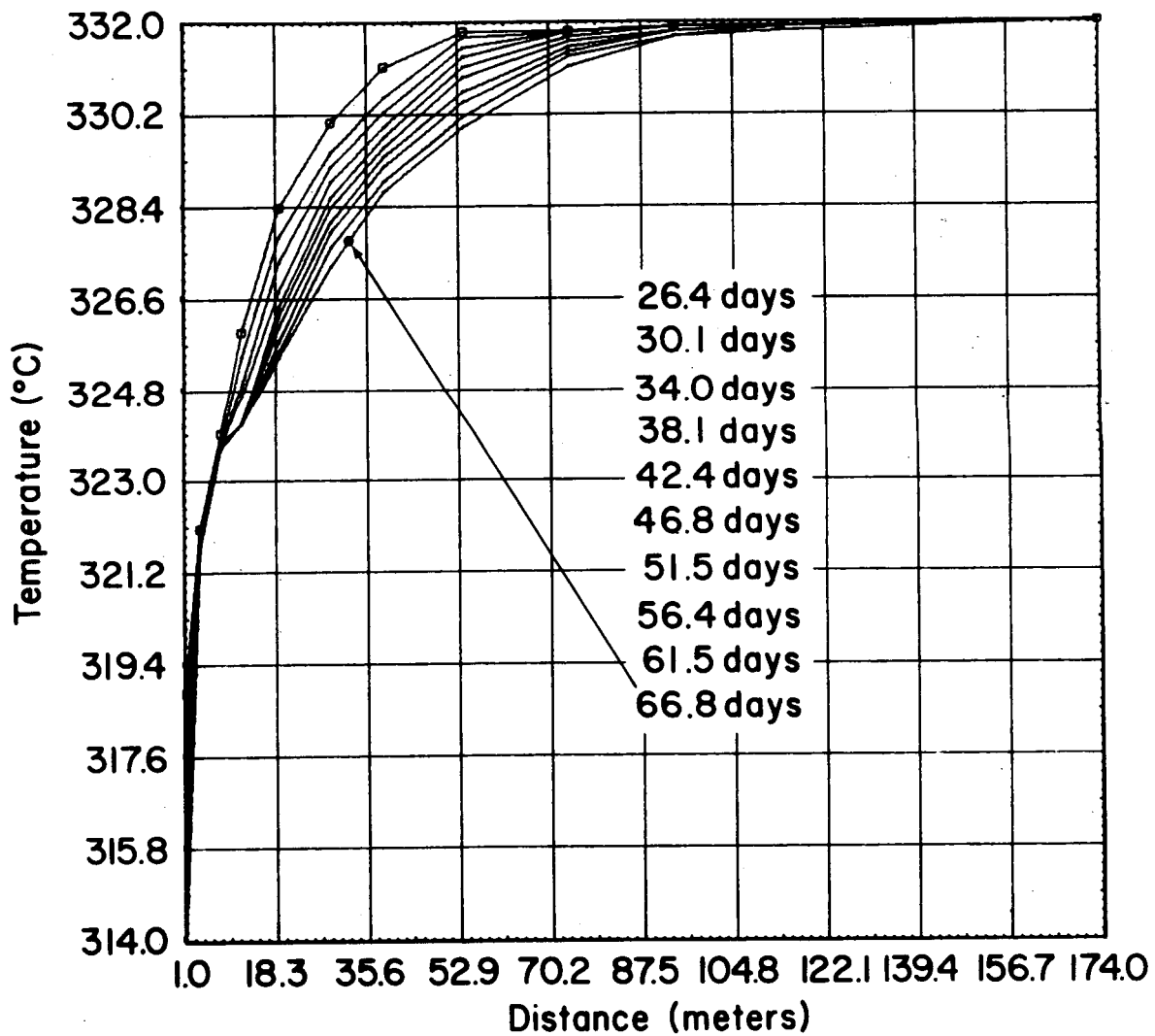
XBL 789-1727

Fig. 26. Pressure drawdown for radial flow, Case 1.2.



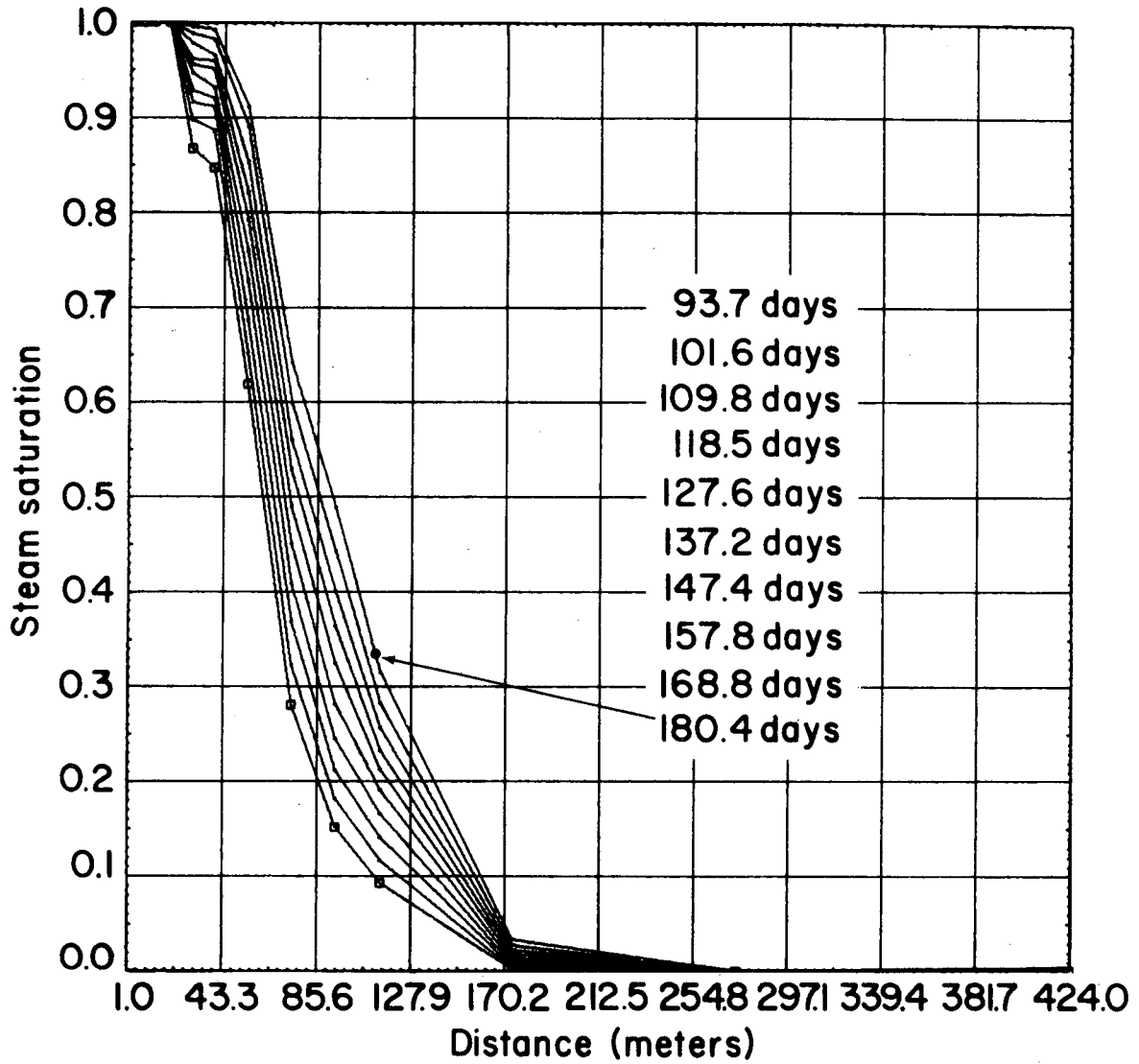
XBL 789-1728

Fig. 27. Pressure drawdown for radial flow, Case 3.2.



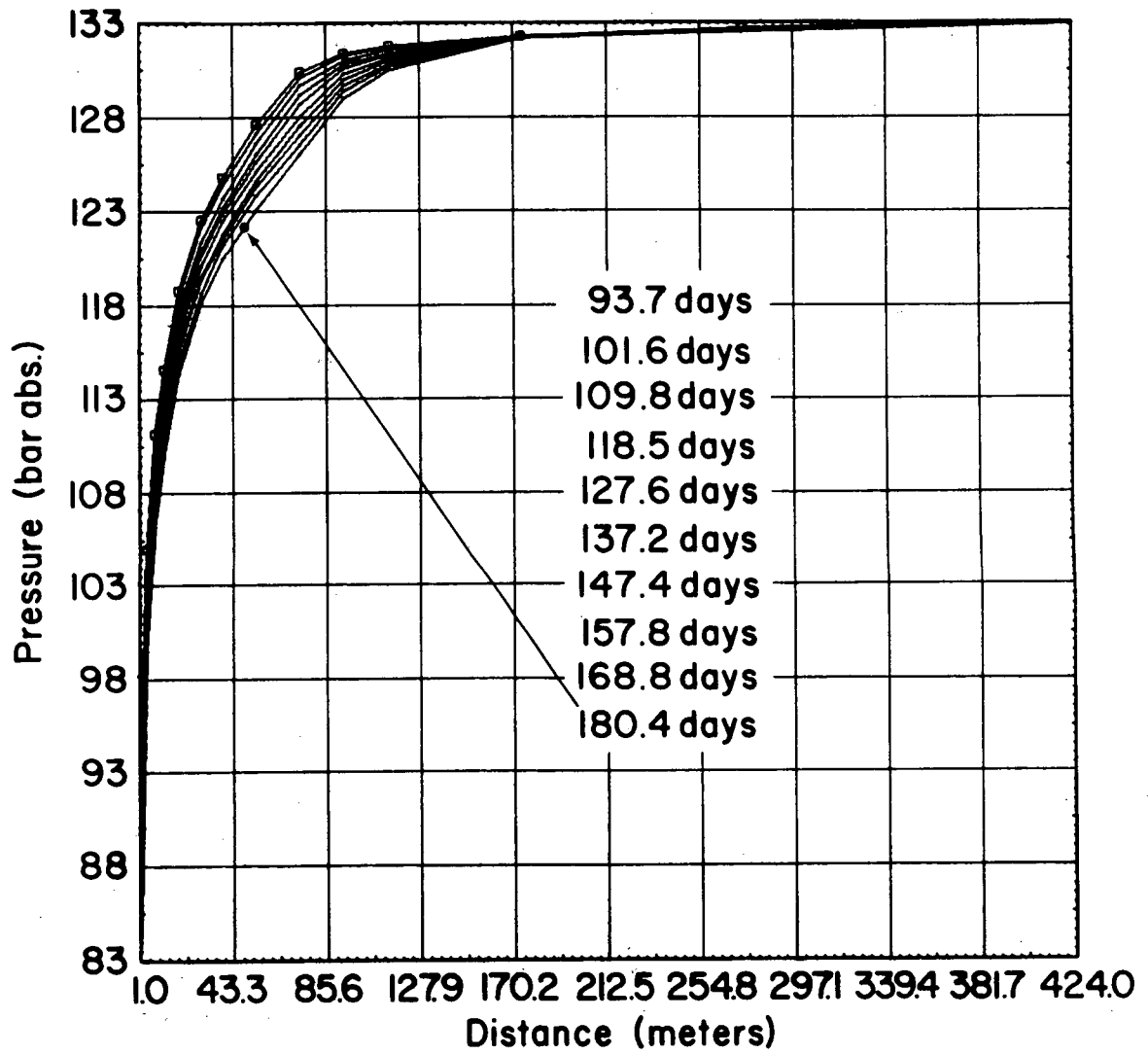
XBL 789-1729

Fig. 28. Temperature depletion for radial flow, Case 3.2.



XBL 789-1730

Fig. 29. Steam saturation for radial flow, Case 1.3.



XBL 789-1731

Fig. 30. Pressure drawdown for radial flow, Case 1.3.

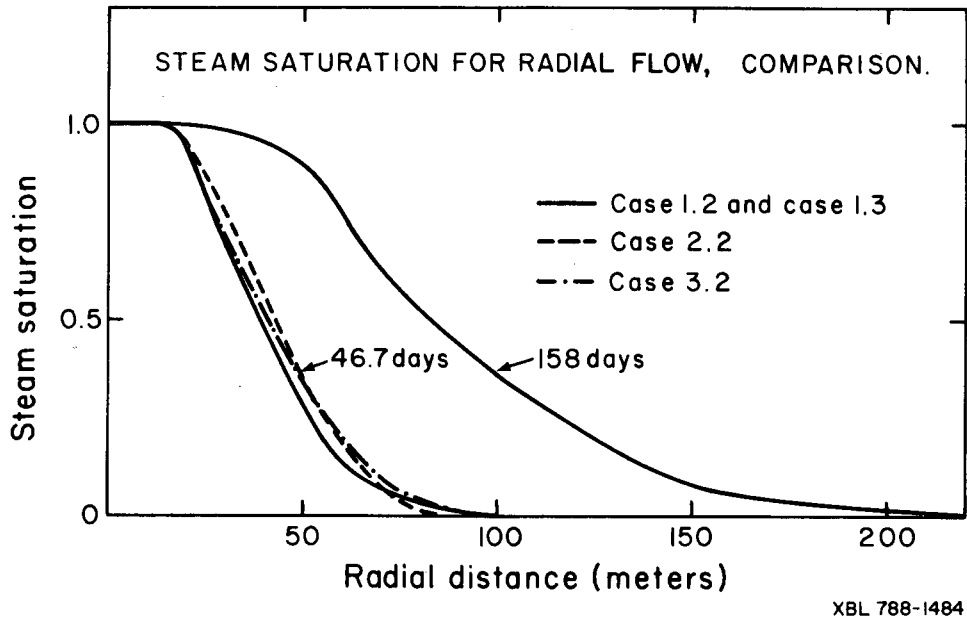


Fig. 31. Steam saturation for radial flow, comparison.

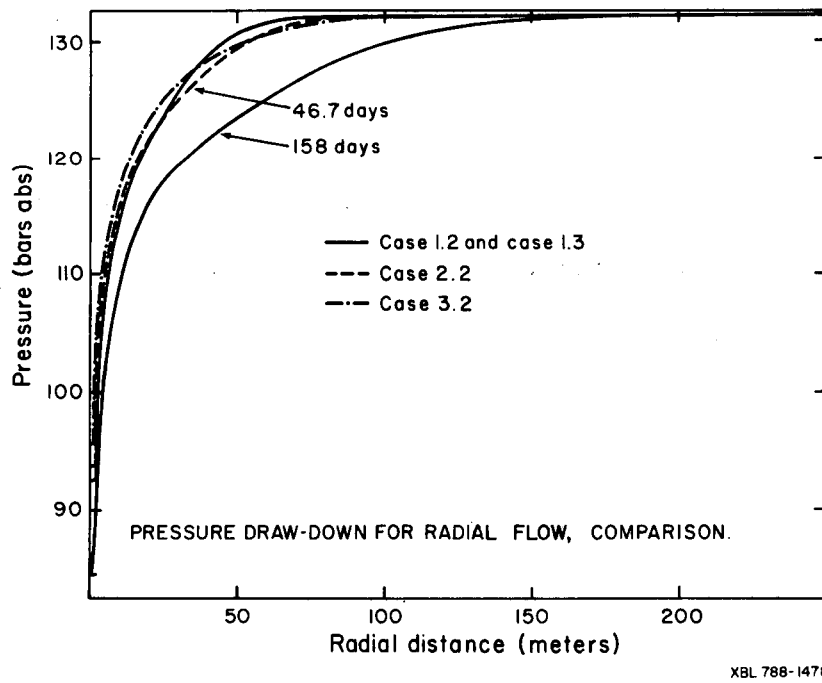


Fig. 32. Pressure drawdown for radial flow, comparison.

Two-Zone Simulation

A two-zone simulation was undertaken in order to understand the interaction between the two zones when fluid withdrawal was made from both zones. A 10° sector was cut out of the geothermal reservoir and studied for a mass flux of 10 kg/s withdrawal from each of three vertical elements at a depth of 1750-2125 meters. Above these elements, at a depth of 875 - 1000m, 20 kg/s was withdrawn from one element, yielding a total withdrawal of 50 kg/s. This would represent typical production for a well in a state undisturbed by the effects of chemical minerals or non-condensable gas. A net inflow equal to 60% of the withdrawal was assumed to flow back into the lower zone of the reservoir, but the upper zone was assumed to replenish its own loss of flow from the bottom layer to the surface equal to 20 kg/s.

The dimensions of the two-zone simulation are shown on Fig. 8. A 500 m thick caprock of practically zero permeability ($k = 10^{-17} \text{ m}^2$) lies between the two zones at a depth of 1000 - 1500 meters, except for the first three elements of the apex which extends 500m in radial distance, and has the same permeability and other properties as the upper zone. Table 3 gives the properties of the rock materials, which are assumed to be independent of temperature.

TABLE 3 - ROCK PROPERTIES

	Density	Porosity	Permeability	Thermal Conductivity	Specific Heat
	kg/m ³	Dimensionless	m ²	W/m-°C	J/kg-°C
Upper Zone	2650	0.10	3.10 ⁻¹⁴	2.9	950
Lower Zone	2560	0.10	1.10 ¹⁴	2.9	950
Caprock	2650	0.01	1.10 ⁻¹⁷	2.9	950

The initial conditions of pressure and temperature are shown in Fig. 6. Constant temperature boundary conditions on top and bottom are imposed by giving the top and bottom layer an artificially high heat capacity, for example 10⁶ J/kg°C. The vertical boundaries of the reservoir are assumed to be adiabatic and impermeable. The inflow mentioned above and the mass withdrawal are treated as mass sources and sinks.

The grid consists of 16 layers, each of 125 meters thickness. In each layer there are 11 elements, giving a total of 176 elements. The computer (CDC 7600) took approximately 0.6 computer seconds to execute a typical energy cycle, but that figure depends on how many flow cycles were executed for each energy cycle. On the average, about 6 flow cycles were done for each energy cycle when the maximum allowable variation in energy change for each time step was $\Delta E \leq 10 \text{ kJ/kg}$, the maximum allowable change in density change for each flow cycle time step was $\Delta \rho \leq 10 \text{ kg/m}^3$, and the maximum allowable pressure change was less than 5 percent of the actual pressure.

When dealing with two-phase flow, in order to accomplish simulation for a reservoir of this size over so many years, it was necessary to increase the value of these parameters, which in turn control the time steps taken. This will hopefully result in no appreciable loss in accuracy regarding the time step.

When dealing with mass sources, the enthalpy of the source must also be given. For the sink term, the enthalpy is easily computed for single phase fluid. For two-phase fluid, the mass fraction of each phase and the total enthalpy must be computed.

In order to consider the horizontal withdrawal out of the element, the combination of Eqs. (1) and (2) gives the quality of the steam defined as the mass of steam withdrawn divided by the total mass withdrawn.

$$x = \frac{F_v}{F_v + F_\ell} = \frac{\rho_v \frac{kR_v}{\mu_v} \Delta P}{\rho_v \left(\frac{kR_v}{\mu_v} + \rho_\ell \frac{kR_\ell}{\mu_\ell} \right) \Delta P} \quad (5)$$

$$x = \frac{\frac{\rho_v R_v}{\mu_v}}{\frac{\rho_v R_v}{\mu_v} + \rho_\ell \frac{R_\ell}{\mu_\ell}} \quad (6)$$

All values on the right hand side of Eq. (6) are the average values in the element and are solved for each time step.

The mass flow for each phase is then given as:

$$\dot{m}_v = x \dot{m}_{\text{sink}} \quad (7)$$

and

$$\dot{m}_\ell = (1-x) \dot{m}_{\text{sink}} \quad (8)$$

The specific enthalpy of the mass flux withdrawn is given by:

$$h = x h_v + (1-x) h_\ell \quad (9)$$

and the total enthalpy flux is:

$$\dot{H} = h \dot{m}_{\text{sink}} \quad (10)$$

The saturation of the sink flow can be higher or lower than the saturation in the element, i.e., more or less steam than water can be withdrawn. The relationship between steam quality and steam saturation is given by the equation:

$$x = \frac{S\rho_v}{S\rho_v + (1-S)\rho_\ell} \quad (11)$$

If this equation is compared with Eq. (6), then the quality of the fluid withdrawn is equal to the quality of the fluid in the cell only when

$$\frac{R_\ell}{R_v} \frac{\mu_v}{\mu_\ell} = \frac{1-S}{S} \quad (12)$$

When the right hand side of Eq. (12) is greater than the left hand side, the quality of fluid withdrawn from the element is less than the quality of the fluid in the element and vice versa.

The SHAFT78 computer program simulated the two-zone reservoir for 33.3 years. This simulation modeled about 1600 energy cycles and about 10,000 flow cycles.

Figure 33 shows the pressure drawdown and saturation as a function of time in the center of the drawdown in the lower zone. The fall in pressure is initially very small. At 0.1 year the pressure has dropped only about 1 bar. As the saturation increases in the cell, the pressure drop increases and reaches a straight line on a logarithmic time scale after about 2 years. During this time, the steam saturation has increased to occupy 25% of the void volume.

Shortly thereafter, the pressure begins to fall faster than the straight line. Since the mobility of water is about 10 times higher than mobility of steam under this condition, additional water flows into the element from neighboring elements at similar saturation levels. This is the reason for the decrease of saturation. But as soon as the saturation begins to decrease, the pressure gradient, which is a function of mobility, also becomes less steep. When the pressure shoots above the straight line, the saturation reaches its minimum. The oscillation of the pressure gradient could easily be caused by numerical inaccuracy, the oscillation in saturation is definitely due to the oscillation in the pressure. Garg (1978) discusses a similar phenomenon, where the saturation reaches a constant value less than 1 which results in a constant total mobility and therefore a constant slope of the pressure gradient on a logarithmic time scale.

Figure 34 shows the temperature and the enthalpy flux calculated from

Eq. (9) for the same element shown in the previous figure. The temperature drops by 16°C over a 30 year period. Due to flashing in the formation, the enthalpy initially increases and reaches its maximum level at approximately the same time the saturation reaches its maximum. After 10 years the enthalpy falls steadily as a result of the drop in temperature. The oscillation in saturation does not affect the enthalpy flux after 10 years, for when mobility is at its minimum, the saturation is at its maximum; therefore, the quality of fluid withdrawn, independent of small fluctuations in saturation, remains practically constant.

Figures 35 and 36 show constant pressure curves in the reservoir after $11\text{-}3/4$ years and $33\text{-}1/3$ years. The heavy lines indicate the area of mass withdrawal from the upper and lower zones. That the dip in the constant pressure line in the upper reservoir is considerably smaller than the dip in the lower zone may be partly a result of higher permeability, but it is also the effect of boiling in the lower zone which causes the total mobility to decrease even further.

Figures 37-41 show constant steam saturation lines in the formation after several periods of production. The flash front is first located in two places around the mass withdrawal at the top of the lower zone near the connection with the upper reservoir (Fig. 37). The fluid from the lower zone rushes to the upper zone, causing the pressure to fall and the fluid to boil. After $7\text{-}1/2$ years (Fig. 38), the two flash fronts have connected and spread out, but there is a low in the saturation between the two boiling areas. Figure 39 shows that boiling is taking place in all of the lower zone after $11\text{-}3/4$ years to a depth of 2000 - 2200 meters. Figure 40 shows a constant saturation after 20 years. The 20 percent saturation front

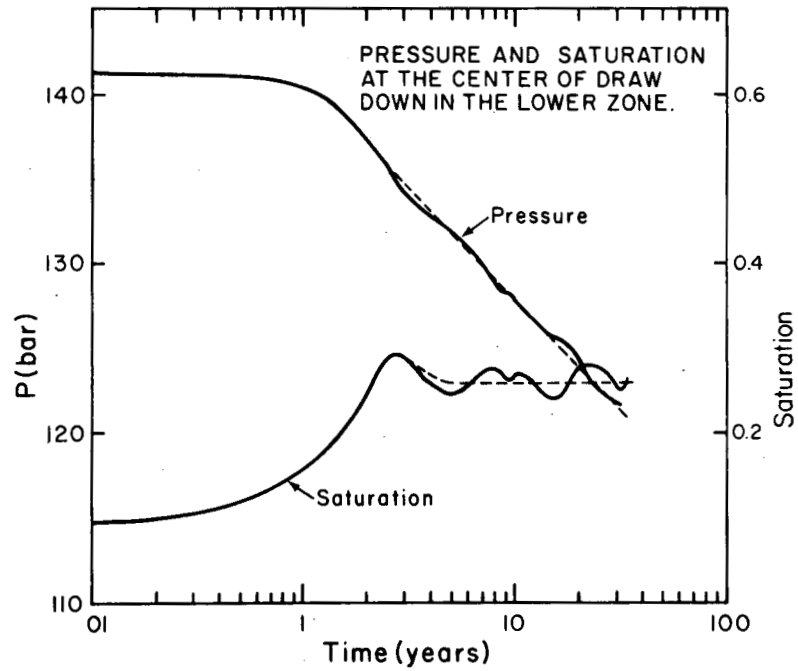
has become larger in both areas, and a 30 percent saturation has occurred in the area connecting the two zones. All the steam that flows upward through the connection condenses as it hits the cold front of the upper zone.

Figure 41 shows the saturation regions at the end of simulation (33-1/3) years. A region 1200 meters wide reaching down to an average depth of 2250 meters is now boiling in the lower reservoir with 60 percent saturation at the top of the zone just under the caprock.

It is expected that this model of the two zones will give a general picture of the reservoir's behavior under conditions of withdrawal. However, because of the very large cells, whose mass sink is equivalent in volume to 130 cubic meters, we lose the degree of resolution for behavior around the borehole which was obtained in the preceding chapter on radial flow. The pressure, temperature and enthalpy flux therefore represent only the average values of the element but not that which can be expected to occur at the borehole itself where all the water has flashed and superheated steam flows from the formation into the borehole. The values of pressure, saturation, temperature and enthalpy flux shown in Figs. 33 and 34 consequently do not represent the values that can be expected to flow into the boreholes. In order to achieve this degree of verisimilitude, the area around boreholes must be simulated by a two-dimensional radial flow superimposed upon the two-zone simulation discussed here.

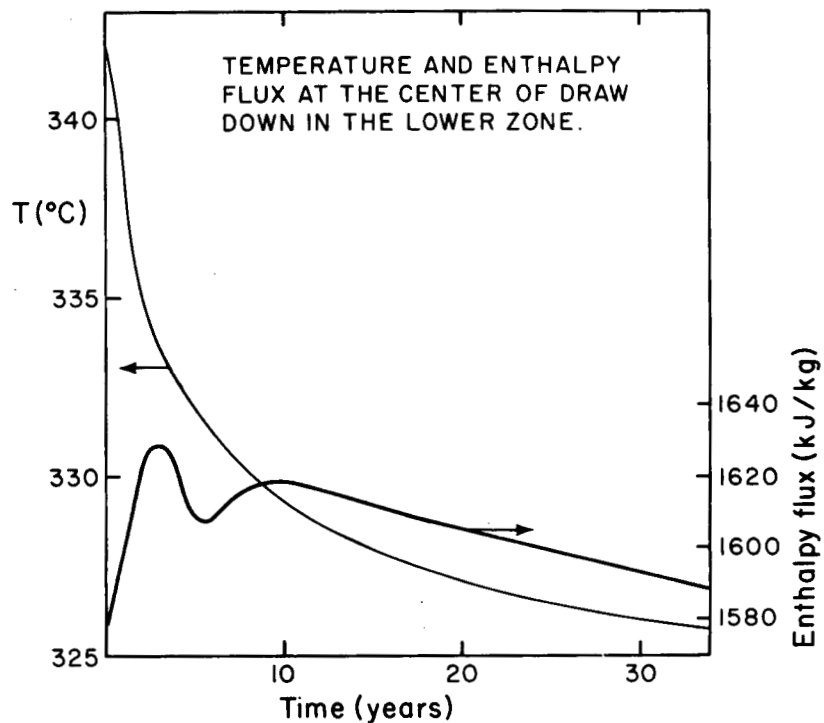
The interesting result of the two-zone simulation is that the entire low-zone of the reservoir is boiling, with steam saturation in the range of 20-60 percent after only a few years of exploitation. If more mass is withdrawn from the lower zone, the time required by the reservoir to reach

an equivalent level of saturation will be inversely proportional to the mass withdrawn. For instance, a 60 kg/s mass production will yield a similar saturation distribution after approximately half the time required for a mass production of 30 kg/s. The pressure distribution will of course be different and depend upon the location of the drawdown.



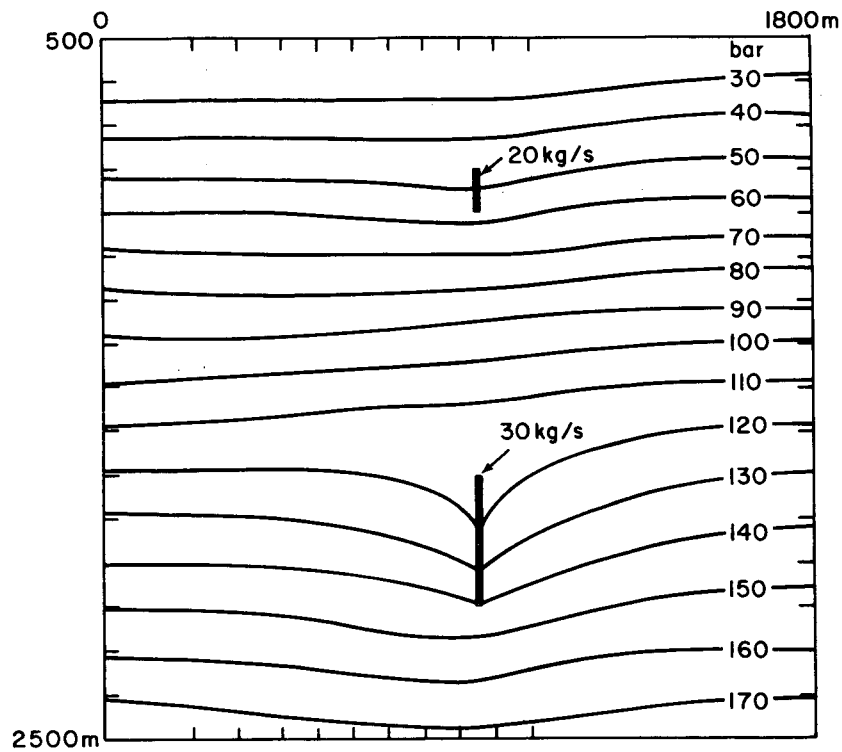
XBL 788-1482

Fig. 33. Pressure and saturation at the center of drawdown in the lower zone.



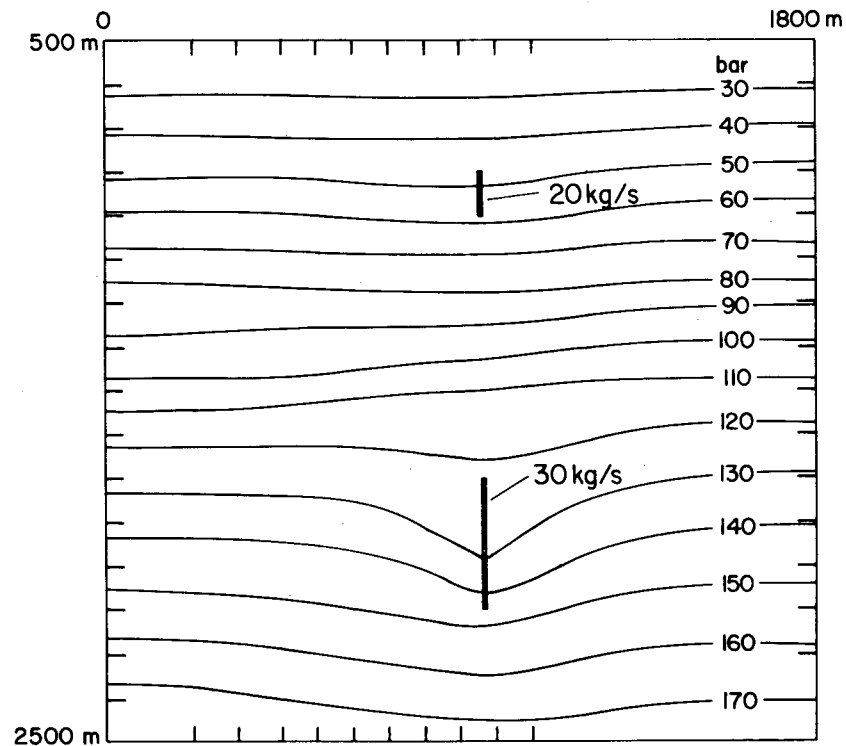
XBL 788-1481

Fig. 34. Temperature and enthalpy flux at the center of drawdown in the lower zone.



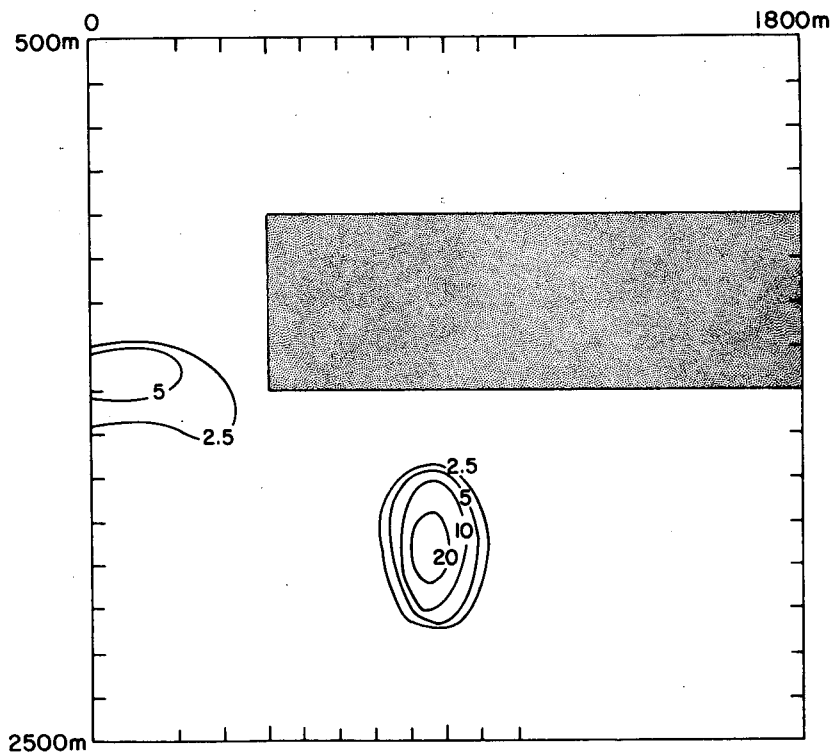
XBL 788-1479

Fig. 35. Pressure distribution in the reservoir after 11-3/4 years of constant production of $\dot{m} = 50$ kg/s.



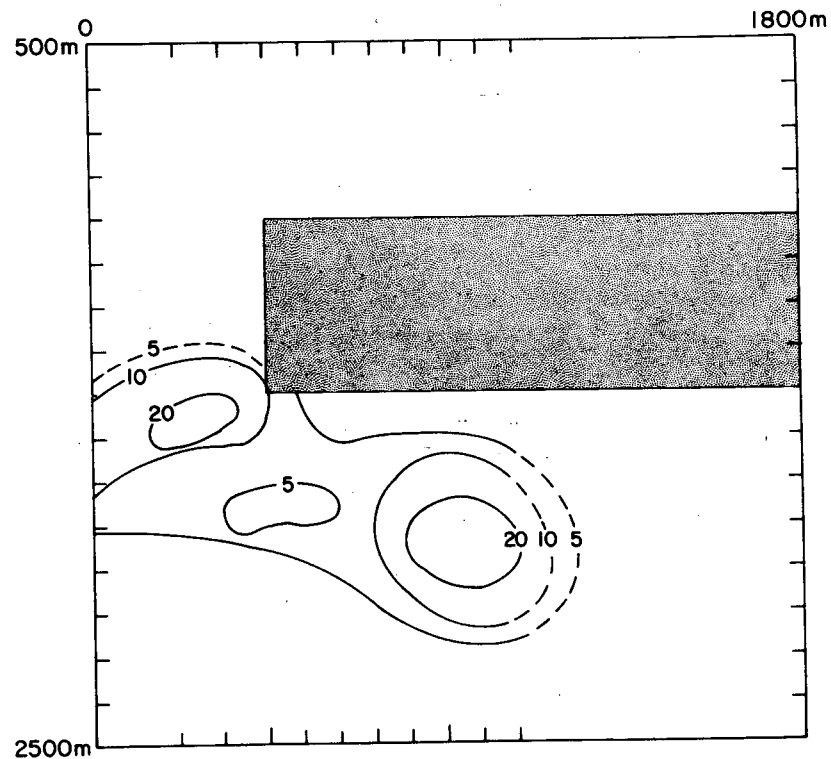
XBL 788-1489

Fig. 36. Pressure distribution in the reservoir after 33-1/3 years of constant production of $\dot{m} = 50$ kg/s.



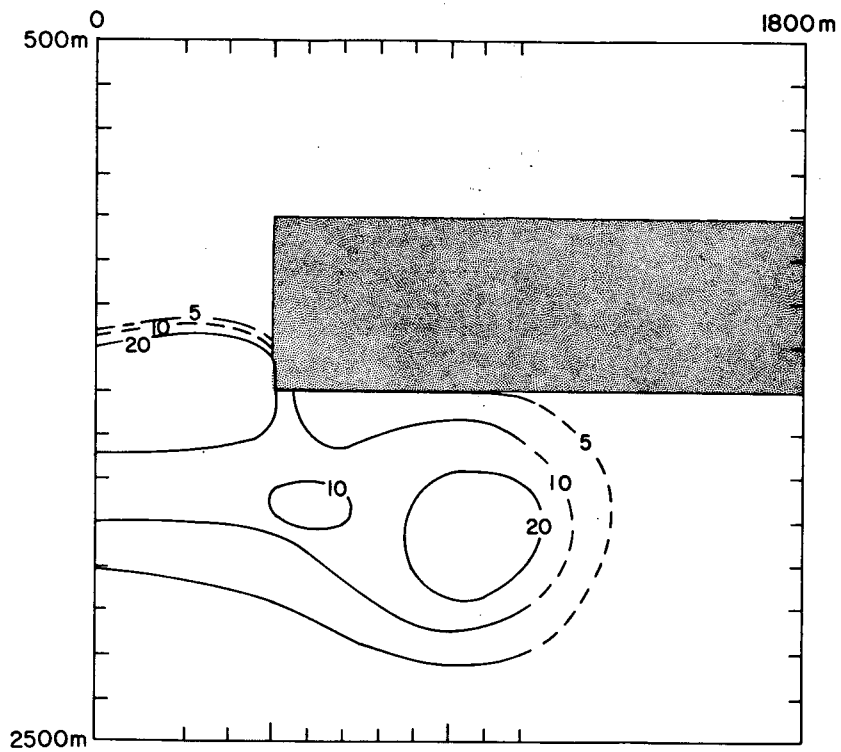
XBL 788-1486

Fig. 37. Pressure distribution in the reservoir after 33-1/3 years of constant production of $\dot{m} = 50$ kg/s.



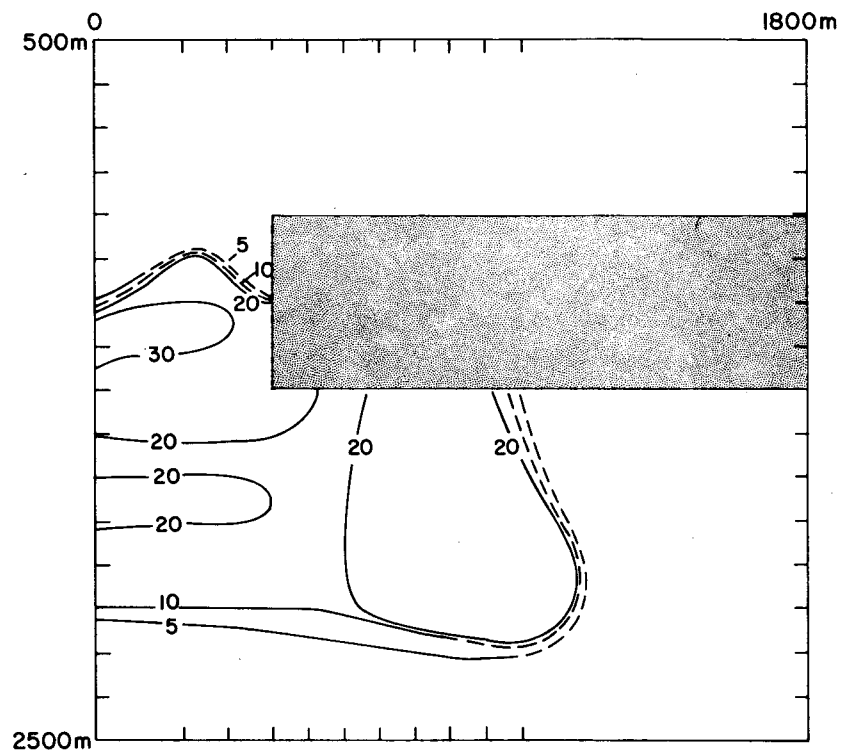
XBL 788-1488

Fig. 38. Steam saturation in formation after 2-1/4 years of constant production of $\dot{m} = 50$ kg/s.



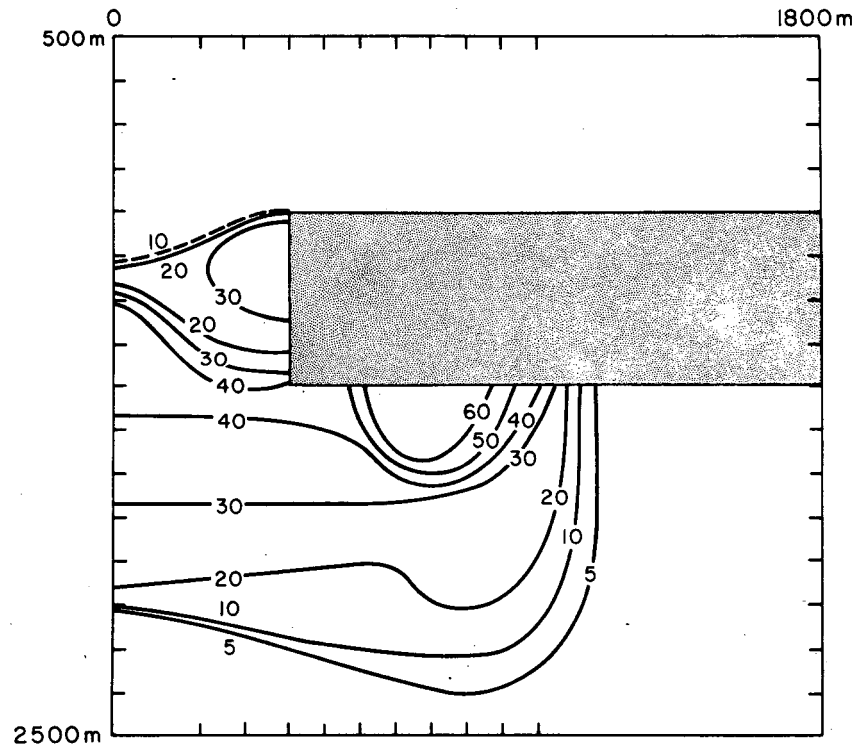
XBL 788-1485

Fig. 39. Steam saturation in formation after 7-1/2 years of constant production of $\dot{m} = 50$ kg/s.



XBL 788-1487

Fig. 40. Steam saturation in formation after 11-3/4 years of constant production of $\dot{m} = 50$ kg/s.



XBL 788-1480

Fig. 41. Steam saturation in formation after 33-1/3 years of constant production of $\dot{m} = 50$ kg/s.

CONCLUSIONS

When a reservoir is close to its saturation point and the absolute permeability of the formation is small, radial flow studies indicate that the fluid in the element containing the production becomes superheated steam very rapidly, in fact, within a few days. The superheated steam zone, however, spreads rather slowly. After 1/2 year of production, it extends less than 20 meters radial distance from the well, while the boiling zone in the formation has spread more than 200 meters in radial distance. The general behavior of the reservoir, e.g., the pressure drop and the spread of the superheated steam front and the boiling front, is only slightly affected by the relative permeability distribution over the wide range of cases studied. No discontinuity of the pressure gradient can be found across the boiling boundaries.

For a two-zone reservoir having an impermeable layer between a cold upper zone and a hot zone near saturation at the bottom, it is seen that boiling in the formation begins not only near the production wells, but it can also begin where the two zones connect. Because the elements considered in the modeling of the two-zone reservoir are so large, no superheated region was found, as was the case in the radial flow study, due to a loss in resolution; but the boiling zone spreads relatively fast, and boiling takes place in the lower zones down to 3200 meters depth long before detection of a superheated steam region. It is believed that boiling will continue to take place in a large portion of the lower zone and not return superheated until most of the formation has become saturated by steam. As indicated by the results, the superheated region will

begin at the top of the lower zone just below the caprock and descend gradually from there.

It would be desirable to continue simulation of the Krafla Geothermal Field in order to consider the total geothermal area under full production corresponding to 60 MW and 120 MW electrical power generation. Such research would superimpose the radial flow upon the large grid near the production wells and would eventually include injection wells located at the edges of the reservoir.

ACKNOWLEDGMENTS

The author wishes to thank many of the researchers at the Earth Sciences Division, LBL. Particular thanks are due to Professor P. Witherspoon and Dr. J. Howard for making this work possible. Dr. R. Schroeder, Dr. K. Pruess and M. Zerzan have offered valuable contributions through discussions and through their assistance in the SHAFT78 computer program simulation. Gudmunder Bodvardsson assisted in the generation of the OGRE computer program grid. The author wants to thank all of these people with gratitude.

NOMENCLATURE

- B mobility, $\frac{\rho k}{\mu}$, seconds
g acceleration of gravity, 9.80665 m/sec²
h specific enthalpy, $u + P/\rho$, kJ/kg
k absolute permeability, m² (1 md=10⁻¹⁵ m²)
k_t thermal conductivity W/m°C
 \dot{m} mass production rate, kg/s
P pressure, bar = 10⁵ N/m²
R relative permeability, dimensionless
r residual immobile water saturation (volume fraction, dimensionless)
S steam saturation (volume fraction), dimensionless
t time: seconds, days, years
T temperature, °C
u specific internal energy, kJ/kg
x quality (mass fraction of steam), dimensionless

Greek

- \emptyset porosity, void fraction
 ρ density, kg/m³
 μ dynamic viscosity, kg/m-s

Subscripts

- ℓ liquid
v vapor

REFERENCES

- Bjornsson, A., Einarsson, P., Grönvold, A., Saemundsson, K., Tryggvason, E., 1977. Current rifting episode in Northern Iceland: *Nature*, v. 266, p. 318-322.
- Bjornsson, A., Johnsen, G., Sigurdsson, S., Thorbergsson, G., Tryggvason, E., 1978. Rifting of the plate boundary in North Iceland, 1975-1978: National Energy Authority (NEA) of Iceland, OS-JHD 7821, and Nordic Volcanological Inst. 7807.
- Chen, Hsiu-Kuo, 1976. Measurement of water in porous media under geothermal fluid flow conditions: Stanford report SGP-TR-15.
- Chen, H. K., Council, J. R., Ramey, N. J., 1978. Experimental steam-water relative permeability curves: Geothermal Resources Council, Transactions, v. 2, p. 103-104.
- Corey, A. T., 1954. The interrelation between gas and oil permeabilities: *Prod. Monthly*, v. 19, p. 38-41.
- Garg, S. K., 1978. Pressure transient analysis for two-phase geothermal reservoir: Geothermal Resources Council, Transactions, v. 2, p. 203-206.
- National Energy Authority (NEA) of Iceland, 1977. Borehole bulletin, No. 7.
- Pruess, K., Schroeder, R. C., Zerzan, M. J., 1978. Studies of flow problems with the simulator SHAFT78: Summaries, Fourth Workshop, Geothermal Reservoir Engineering, Stanford University, Dec. 13, 1978.
- Pruess, K., Zerzan, J. M., Schroeder, R. C., Witherspoon, P. A. 1979. Description of the three-dimensional two-phase simulator SHAFT78 for use in geothermal reservoir studies: Society of Petroleum Engineers of AIME 5th Symposium on Reservoir Simulation, Denver, Colorado, Feb. 1-2, 1979: SPE-7699. Lawrence Berkeley Laboratory Preprint: LBL-8802.
- Saemundsson, K., 1974. Evolution of the axial rifting zone in Northern Iceland and the Tjornes fracture zone: *Geol. Soc. Am. Bull.*, v. 85, No. 495.
- Sugurdsson, O., Stefansson, V., 1977. Transmissivity in boreholes in Krafla: NEA of Iceland, OS-JHD 7727.
- Weres, O., Schroeder, R., 1978. Documentation for program OGRE: Lawrence Berkeley Laboratory report, LBL-7060.

This report was done with support from the Department of Energy. Any conclusions or opinions expressed in this report represent solely those of the author(s) and not necessarily those of The Regents of the University of California, the Lawrence Berkeley Laboratory or the Department of Energy.

Reference to a company or product name does not imply approval or recommendation of the product by the University of California or the U.S. Department of Energy to the exclusion of others that may be suitable.

TECHNICAL INFORMATION DEPARTMENT
LAWRENCE BERKELEY LABORATORY
UNIVERSITY OF CALIFORNIA
BERKELEY, CALIFORNIA 94720